

## Article

# Modification of Polylactide-poly(butylene adipate-co-terephthalate) (PLA/PBAT) Mixed-Matrix Membranes (MMMs) with Green Banana Peel Additives for Oil Wastewater Treatment

Maryam Y. Ghadhban<sup>1</sup>, Khalid T. Rashid<sup>1</sup>, Adnan A. Abdulrazak<sup>1</sup> , Israa Taha Ibrahim<sup>2</sup>, Qusay F. Alsahy<sup>1</sup> , Zaidoon M. Shakor<sup>2</sup>  and Ihsan Hamawand<sup>3,\*</sup>

<sup>1</sup> Membrane Technology Research Unit, Chemical Engineering Department, University of Technology, Al-sinaa Street 52, Baghdad 10066, Iraq; maryam.y.ghadhban@uotechnology.edu.iq (M.Y.G.); khalid.t.rashid@uotechnology.edu.iq (K.T.R.); adnan.a.alsalim@uotechnology.edu.iq (A.A.A.); qusay.f.abdulhameed@uotechnology.edu.iq (Q.F.A.)

<sup>2</sup> Department of Forensic Science, College of Science, Al-Karkh University of Science, Baghdad 10066, Iraq; dr.israa.taha@kus.edu.iq (I.T.I.); zaidoon.m.shakor@uotechnology.edu.iq (Z.M.S.)

<sup>3</sup> Wide Bay Water Process Operations, Fraser Coast Regional Council, Urangan, QLD 4655, Australia

\* Correspondence: ihsan.hamawand@gmail.com; Tel.: +61-0466897659

**Abstract:** Ultrafiltration membranes are often considered a highly efficient technique for purifying oily wastewater. The primary objective of this research was to improve the performance and antifouling properties of PLA/PBAT membranes used in oily wastewater treatment by incorporating banana peel (BP) nanoparticles. Various characterization techniques, including field emission scanning electron microscopy (FESEM), wettability analysis, pure water flux measurement, porosity assessment, tensile analysis, and FTIR analysis, were employed to describe the prepared membranes. The results of the FT-IR test revealed that BP nanoparticles were effectively integrated into the PLA/PBAT membrane matrix. The contact angle decreased from 73.7° for the pristine PLA/PBAT membrane to 38.99° for the membrane incorporating 0.05 wt.% BP-NPs, indicating that the nanoparticles enhanced the hydrophilic characteristics of the membranes. A similar trend was observed for the pure water flux of PLA/PBAT/BP membranes, suggesting that membranes with a BP-NP concentration of 0.05 weight percent exhibited the highest pure water flux. This improvement can be attributed to the synergistic effects of the nanoparticles. Additionally, the presence of BP-NPs enhanced the mechanical properties of the membranes. Finally, an ultrafiltration system using oily wastewater as feed was employed to evaluate the performance of the prepared membranes. The finding demonstrated that PLA/PBAT/BP membranes exhibited a higher flux and a greater oil removal efficiency of 105.3 L/m<sup>2</sup>h and 95.2% compared to neat PLA/PBAT membranes (62 L/m<sup>2</sup>h and 88%), respectively.

**Keywords:** ultrafiltration; PLA/PBAT membranes; banana peel nanoparticles (BP-NPs); antifouling; oily wastewater treatment



**Citation:** Ghadhban, M.Y.; Rashid, K.T.; Abdulrazak, A.A.; Ibrahim, I.T.; Alsahy, Q.F.; Shakor, Z.M.; Hamawand, I. Modification of Polylactide-poly(butylene adipate-co-terephthalate) (PLA/PBAT) Mixed-Matrix Membranes (MMMs) with Green Banana Peel Additives for Oil Wastewater Treatment. *Water* **2024**, *16*, 1040. <https://doi.org/10.3390/w16071040>

Academic Editor: John Zhou

Received: 5 February 2024

Revised: 28 March 2024

Accepted: 29 March 2024

Published: 4 April 2024



**Copyright:** © 2024 by the authors. Licensee MDPI, Basel, Switzerland. This article is an open access article distributed under the terms and conditions of the Creative Commons Attribution (CC BY) license (<https://creativecommons.org/licenses/by/4.0/>).

## 1. Introduction

The most widespread source of global water pollution is oil discharge from oil fields, typically ranging from 100 to 1000 ppm [1]. Effective treatment and removal of oily pollutants are essential for pollution management, with environmental standards requiring oil and grease concentrations in wastewater to be maintained below 10–15 mg/L [2].

Oily wastewater is a residual byproduct found in various industries, including food manufacturing, petrochemical plants, pharmaceuticals, and oil refineries [3]. Existing methods for separating oil-in-water mixtures, such as gravity separation, air flotation, adsorption, flocculation, and coagulation, often prove insufficient for emulsions with oil droplets as small as 0.1 µm [4].

The membrane technique has gained prominence for its ability to effectively separate stabilized oil/water emulsions. It offers advantages such as simplicity, quick processing, minimal space requirements, and high separation efficiency [5,6]. However, commonly used hydrophobic membrane materials like poly (vinylidene fluoride) and polysulfone cannot be easily biologically degraded, posing a risk of secondary contamination [7]. To address this, researchers have sought eco-friendly alternatives, and polylactic acid (PLA) has emerged as a promising biodegradable material [8,9].

Membrane fouling, caused by oil molecule accumulation, remains a significant concern for long-term operations. Hydrophilic membranes with pore sizes smaller than oil droplet diameters have been developed to combat fouling [10,11]. Previous research has focused on surface modifications and the incorporation of hydrophilic additives to enhance fouling resistance [12,13].

For instance, Liu et al. created a polylactide membrane embedded with TiO<sub>2</sub> nanoparticles, achieving a high water flux of 950 L/m<sup>2</sup>h and 99% oil rejection [14]. Ismail et al. improved membrane performance by adding hydrous manganese oxide (HMO) nanoparticles to polyvinylidene fluoride (PVDF), achieving a pure water flux ten times higher than pristine PVDF membranes with 93% oil rejection [15].

Recent trends in membrane development emphasize not only performance improvement but also eco-friendly design practices. Researchers are exploring environmentally friendly solvents, additives, and polymers sourced from biological origins [16–18].

In recent years, there has been growing interest in using green additives derived from plant waste or sustainable resources. These additives are environmentally friendly, readily available, and cost-effective. They offer versatility in nanoparticle production for membrane manufacturing, promoting sustainability [19,20]. For example, mingliang et al. developed a mullite ceramic membrane with recycled materials to separate oil-in-water emulsions [21]. Other studies have successfully utilized waste materials like corn straw and potato peel for selective oil/water separation [22–24]. Additionally, banana peel has been employed for various environmental applications [25]. For instance, Poonam used wasted banana peel as a biodegradable resource for manufacturing an ionic polymer membrane. Different studies have used green banana peel extract to fabricate membranes and showed promise in repairing epithelial lesions [26,27].

In this study, we modified PLA/PBAT membranes using green-banana-peel-derived nano particle (BP-NP) additives. Our investigation aims to assess how varying concentrations of BP-NPs affect the performance and morphology of the modified membranes, including structural features, porosity, pore size, contact angle, and functional group analysis. We evaluated the membrane's performance in the removing of diesel oil from wastewater solutions. What makes this study unique is that it looks at the potential impact of green additives (BP) on the equilibrium characteristics of the PLA/PBAT membrane in the removal of oil in oil/water emulsion.

## 2. Methodology

### 2.1. Materials and Chemicals

Dichloromethane (DCM) was sourced from the German company Merck KGaA, Darmstadt, Germany. Sodium Decyl Sulfate (SDS) was procured from HIMEDIA in Mumbai, India. PLA with a molecular weight of 80,000 and PBAT with a molecular weight of 120,000 were acquired from Hubei Bluesky New Material Inc. Co. in Wuhan, China. The bananas were obtained from a local market in Baghdad, Iraq. Diesel oil was supplied by Al-Daura Refinery, also located in Baghdad, Iraq.

### 2.2. Green Banana Peel (BP) Powder Preparation

The banana peels were separated from the fruits, thoroughly cleaned with distilled water to remove any dirt, sliced into small pieces, and then dried in an oven at 65 °C for 48 h. After drying, the banana peel was ground into a powdered form using nano milling. Subsequently, the powdered peels were sieved to achieve a uniform particle size. To ensure

complete removal of any remaining moisture, the powdered banana peels underwent an additional drying step in an oven set at 65 °C for 6 h. The dried powder was stored in a plastic container at room temperature until it was ready for use.

Furthermore, FT-IR was used to analyze chemical structures and identify functional groups. Figure 1A depicts the chemical structure of the banana peel [27].

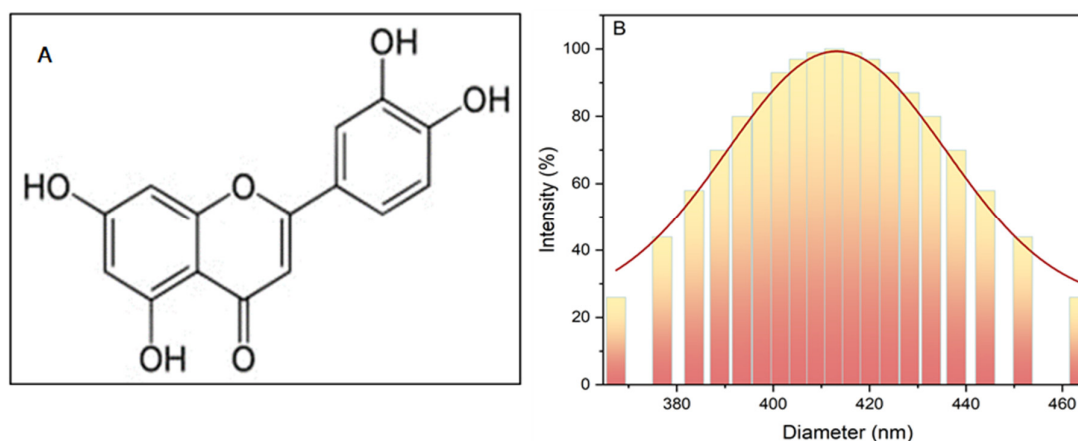


**Figure 1.** Banana peel (A) chemical structure; (B) dynamic light scattering of the particle size.

The particle size of the powder was determined using dynamic light-scattering analysis (DLS) with a device from Brookhaven Instruments Corporation, Holtsville, NY, USA, revealing an average diameter of approximately 400 nm, as illustrated in Figure 1B.

### 2.3. Preparation of (PLA/PBAT/BP) Membranes

Initially, various quantities of BP nanoparticles, including concentrations of 0%, 0.0125%, 0.025%, 0.05%, and 0.1% by weight, were introduced into Dichloromethane (DCM). Following this, the mixture underwent ultrasonication for 1 h to ensure even distribution of additives and prevent agglomeration. Subsequently, a solution comprising 14% PLA and 4% PBAT was added to the mixture while vigorously stirring in a covered flask for 12 h, achieving a uniform solution. The addition of these two components was carefully controlled to prevent accumulation. The resulting homogeneous solution underwent sonication to eliminate any bubbles, as the presence of bubbles could compromise membrane quality. The same procedure was repeated for producing PLA and PBAT membranes without BP additives. Table 1 provides details of the components used in the nanocomposite membranes.

**Table 1.** The composition of PLA/PBAT/BP membrane.

Sample	PLA (wt.%)	PBAT (wt.%)	BP (wt.%)	Solv. (wt. %)
MB1	14	4	0	82
MB2	14	4	0.0125	82
MB3	14	4	0.025	82
MB4	14	4	0.05	82
MB5	14	4	0.1	82

The fabrication of flat sheet membranes followed the phase-inversion method. A high-quality solution was applied onto a clean glass plate, and a mechanized knife with a 150 µm gap was employed to cast the flat sheet membrane. After 4 min of evaporation, the glass plate with the formed membrane was immersed in water to facilitate its natural detachment from the glass surface. Subsequently, it was transferred to another bath of coagulation water to completely remove any remaining solvents. The membranes were then placed in containers filled with deionized (DI) water and left at room temperature until further analysis.

#### 2.4. Preparation of Oily Wastewater Feed Solution

A mixture consisting of diesel oil, distilled water, and sodium dodecyl sulfate (SDS) was prepared to create oil-in-water feed solutions with concentrations of 100, 200, and 300 ppm. The surfactant SDS was utilized to establish emulsion stability for the oil-in-water mixture, maintaining a weight ratio of 10:1 for diesel oil to SDS [28]. The preparation of synthetic oil-in-water emulsions was carried out using a mechanical mixer, specifically the Crown Professional homogenizer, operating at a speed of 12,000 rpm for approximately 15 min at room temperature. This process yielded a uniformly mixed, milky-colored fluid. The mean size of oil droplets within the resulting emulsion of oily wastewater was determined using dynamic light-scattering (DLS) analysis equipment (Brookhaven Instruments Corp., Holtsville, NY, USA), revealing an average diameter of approximately 49 nm.

#### 2.5. The Characteristics of Membranes

To analyze the functional group properties of banana peel (BP) and membranes, Fourier-Transform Infrared Spectroscopy (FT-IR) was employed using an FTIR instrument (SHIMADZU, Kyoto, Japan, IR Affinity-1) from Japan. The data were recorded over a spectrum of frequencies ranging from  $500\text{ cm}^{-1}$  to  $4000\text{ cm}^{-1}$ .

Surface and cross-sectional examination of PLA/PBAT and PLA/PBAT/BP membranes was conducted using a field emission scanning electron microscope (model Inspect-F50) manufactured by ELEMCI in Estepona, Spain. For imaging preparation, the membranes underwent fracturing through exposure to liquid nitrogen and were subsequently coated with a thin layer of gold film using sputtering.

Porosity calculations were performed employing Equation (1). Initially, the membranes were subjected to a drying process at  $45\text{ }^{\circ}\text{C}$  for 12 h to eliminate any remaining moisture. Subsequently, the membranes were weighed, and this measurement was designated as  $W_1$ . After that the dried membrane was soaked in water for one day and then removed from the water, any residual water droplets were carefully removed, and their weight ( $W_2$ ) was measured. Equation (1) was applied to the collected data, and three iterations of the technique were performed to calculate mean values [29]:

$$\varepsilon(\%) = \frac{W_2 - W_1}{Al\rho} \times 100\% \quad (1)$$

In the provided equation above:

$A$  represents the membrane area;

$\rho$  represents the water density;

$l$  represents the thickness of the membrane.

Additionally, the mean pore radius of the membrane can be determined using the filtration velocity technique, as outlined in the Gue–Elford–Ferry equation (Equation (2)) [30]:

$$R_m = \sqrt{\frac{(2.9 - 1.75\varepsilon) \times 8\eta LQ}{\varepsilon \times A \times \Delta P}} \quad (2)$$

In the provided equation above:

$R_m$  represents the mean pore radius of the membrane (measured in meters, m);

$\eta$  represents the viscosity of water;

$Q$  represents the volume of pure water permeated per unit of time;

$L$  represents the membrane thickness (measured in meters, m);

$A$  represents the active membrane area (measured in square meters,  $\text{m}^2$ );

$\Delta P$  represents the operating pressure (measured in Pascals, Pa).

Surface wettability was evaluated using the sessile drop technique and static contact angle measurement equipment (110-O4W CAM) from Tainan, Taiwan. The average contact angle was calculated based on measurements from at least three distinct samples, each prepared separately. To analyze the highly hydrophilic surfaces of the modified membranes,

small strips (1 × 4 cm) of the membrane samples were cut and attached to a glass microscope slide using double-sided tape to create a flat viewing area. Subsequently, the glass slide was placed on a stage, and a 3.5 µL deionized water droplet was dispensed from a syringe onto the top of the membrane. The contact angle (CA) of the water droplet on the flat surface was then measured [31].

Tensile strength measurements were conducted using standardized electronic tensile testing equipment (CO-LTP-WDW-50) from Beijing, China, which was connected to computer software. The samples were uniformly cut into standard strips measuring 20 mm × 100 mm. During testing, the crosshead speed was set to 5mm/min, and the results were recorded accordingly [32].

## 2.6. Membrane Performance

Both the modified and unmodified membranes were assessed for their performance by measuring the flux of pure water, the flux of oil/water, and oil rejection using a crossflow filtering system at room temperature, as illustrated in Figure 2. Prior to conducting the permeation evaluation, the membrane was initially pressurized to 2 bars for half an hour until a stable flux was established. It was then dropped to the transmembrane pressure and water flux was measured for each membrane; information was taken at 10 min intervals. Pure water flux was evaluated following Equation (3) [33]:

$$J = \frac{Q}{At} \quad (3)$$

In the above equation provided:

$J$  represents the permeate flux (measured in kg/m<sup>2</sup>·h);

$A$  represents the effective membrane area (measured in square meters, m<sup>2</sup>);

$Q$  represents the total collected permeate volume (measured in liters, L);

$t$  represents time (measured in hours, hr).

The data presented are an average obtained from a minimum of three independent trials.

After completing the pure water flux (PWF) experiment, the membranes were subjected to an oil/water separation experiment using a similar setup. Similarly, the membranes underwent compaction during the oil/water separation experiment to achieve a stable flux condition. The flux and rejection (%) of the membranes were subsequently calculated using Equations (3) and (4) [34,35]:

$$Rejection\% = \left(1 - \frac{C_p}{C_f}\right) \times 100\% \quad (4)$$

In the provided above equation:

$C_p$  represents the concentration of oil in the permeate;

$C_f$  represents the concentration of oil in the feed.

To assess the oil recovery from both the feed solution and permeate, an oil content analyzer from HORIBA in Kyoto, Japan was used.

To evaluate the influence of experimental variables on oil rejection, the filtration procedure was carried out under the following conditions: a temperature of 25 ± 3 °C, pressure variations across the membrane (1.5, 2.5, and 3.5 bar), and an oil/water concentration ranging from 100 to 300 ppm.

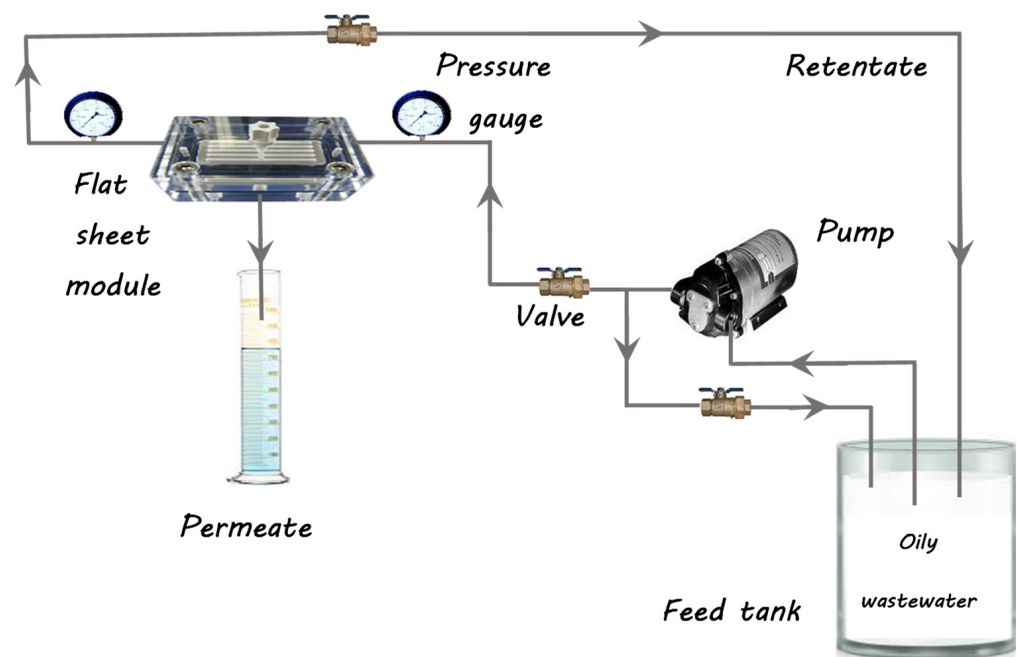


**Figure 2.** A crossflow filtering system.

The antifouling characteristics of both the PLA/PBAT membrane and PLA/PBAT/BP membrane were assessed and compared through the following steps: first, the pure water flux through all membranes was determined. Next, the flux of the permeate (oil/water) solution was measured. Subsequently, after each testing cycle, the fouled membranes underwent a process of backwashing using distilled water for a duration of 1 h. Following the backwashing, the permeate water flux (PWF) of the cleaned membrane was evaluated.

The flux recovery ratio (*FRR*) and total resistance (*R<sub>t</sub>*) were then estimated. The total resistance (*R<sub>t</sub>*) can be further divided into two components: reversible fouling resistance (*R<sub>r</sub>*) and irreversible fouling resistance (*R<sub>ir</sub>*). These calculations were performed using Equations (5)–(8) as appropriate [36]:

$$FRR\% = \left( \frac{J_2}{J_1} \right) \times 100\% \quad (5)$$

$$R_t\% = \left( 1 - \frac{J_p}{J_1} \right) \times 100\% \quad (6)$$

$$R_r\% = \left( \frac{J_2 - J_p}{J_1} \right) \times 100\% \quad (7)$$

$$R_{ir}\% = \left( \frac{J_1 - J_2}{J_1} \right) \times 100\% \quad (8)$$

In the above provided equations:

*J<sub>1</sub>* represents the initial flux of pure water (measured in L/m<sup>2</sup>h) before fouling;

*J<sub>2</sub>* represents the flux of pure water (measured in L/m<sup>2</sup>h) after fouling;

*J<sub>p</sub>* represents the permeate flux of oil/water (measured in L/m<sup>2</sup>h).

### 3. Results and Discussion

#### 3.1. Membrane Characteristic

##### 3.1.1. FT-IR Analysis

Fourier Transform Infrared Spectroscopy (FTIR) is a powerful technique for analyzing chemical structures and identifying functional groups present on membrane surfaces [37]. FTIR spectra of BP-NPs, PLA/PBAT, and modified membranes containing 0.05 wt.% banana

peel powder were collected within the spectrum ranging from  $4000\text{ cm}^{-1}$  to  $500\text{ cm}^{-1}$ . The spectral data were analyzed, and the results are presented in Figure 3.

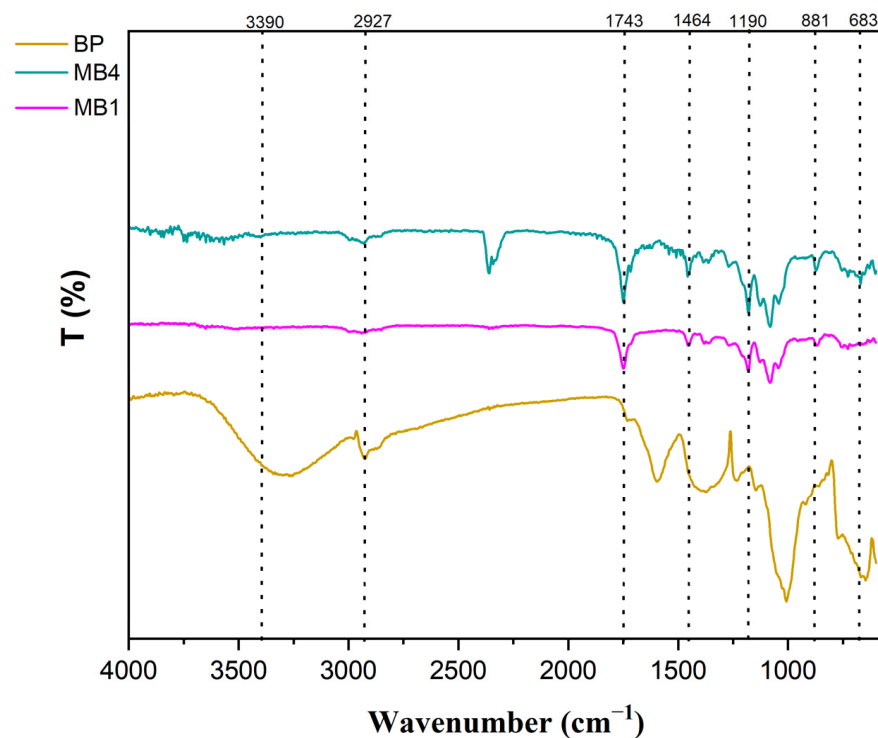


**Figure 3.** FTIR for BP-NPs, PLA/PBAT and PLA/PBAT/BP membranes.

Previous research on banana peel (BP) has indicated the presence of various polymers, including pectin, lignin, and hemicelluloses, which contain abundant organic compounds with functional groups such as  $-\text{NH}_2$ ,  $\text{O-H}$ , and  $-\text{COOH}$  [38,39]. A comparison between the unmodified (PLA/PBAT) membrane and the PLA/PBAT/BP membrane reveals additional absorption peaks in the latter's curve. The peak observed at  $3390\text{ cm}^{-1}$  corresponds to the  $\text{O-H}$  stretching vibration, which is a characteristic absorption peak [40]. The peak at  $2927\text{ cm}^{-1}$  corresponds to the vibrational stretching of the  $\text{C-H}$  bonds. These findings suggest that BP-NPs exhibit activity within the PLA/PBAT casting solution and result in increased surface hydrophilicity in the blended membrane. The presence of peaks at  $1464\text{ cm}^{-1}$  may be attributed to the asymmetric stretching of a phenol group. In addition, the FTIR spectrum of MB4 shows an ambient  $\text{CO}_2$  peak at around  $2366\text{ cm}^{-1}$ . Consequently, it can be inferred that the presence of these peaks provides evidence for the incorporation of BP-NPs, which enhances the hydrophilicity of the modified PLA/PBAT membrane.

### 3.1.2. FE-SEM Test

Field emission scanning electron microscopy (FESEM) was employed to examine the morphological changes resulting from the incorporation of BP-NPs into the casting solution. The analysis focused on both surface and cross-sectional views. Figure 4 displays the FESEM images of the PLA/PBAT membrane, including its top surface, and modifications made using varying amounts of BP-NPs, ranging from 0.0125 to 0.1 weight percent.

The FESEM image of the PLA/PBAT membrane (Figure 4 (MB1)) revealed a flat, uniformly compact, and smooth surface. The introduction of BP-NPs at a very low concentration of 0.0125 wt.% did not significantly affect the flat-sheet membrane's surface, as shown in Figure 4 (MB2). However, a noticeable change in the top surface occurred when the loading ratio was increased to 0.025 wt.% (Figure 4 (MB3)). As the BP concentration continued to increase from 0.05 to 0.1 wt.%, distinct alterations in the membrane's surface morphology were observed, as depicted in Figure 4 (MB4) and (MB5).

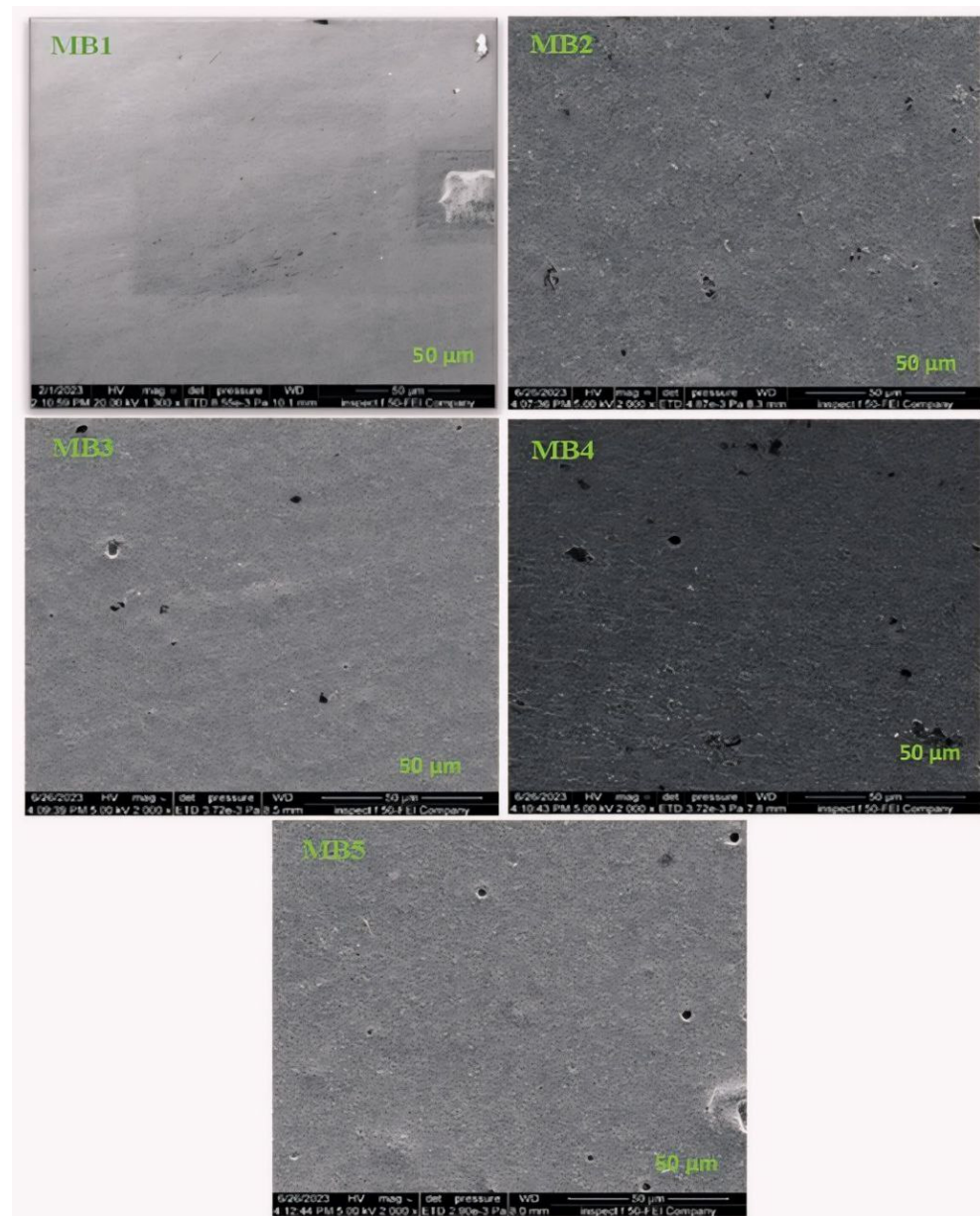


**Figure 4.** FESEM top surface images for the PLA/PBAT/BP membranes.

These analyses illustrate the influence of BP concentration on the compatibility of PLA/PBAT mixed membranes. The observed morphological changes with increasing nano-additive concentration can be logically explained, as a higher BP concentration may lead to an increase in the casting solution's viscosity [17,41]. The increased viscosity of the casting solution may reduce the extent of mixing, and phase separation between the solvent and nonsolvent occurs to a greater extent [42].

The influence of the BP-NP concentration on the cross-sectional morphology of the "PLA/PBAT/BP" blended membrane is depicted in Figure 5. The PLA/PBAT membrane, as shown in Figure 5 (MB1), exhibited a homogeneous and symmetrical spongy-like structure throughout its cross-section, extending from the highest to the lowest point. A very thin active layer was observed on the upper surface of the membrane. Upon adding 0.0125 weight percent of BP to the casting solution, significant structural changes were evident, as depicted in Figure 5 (MB2). With an increase in the BP content within the membrane matrix, the cross-section displayed higher density characterized by larger

and less frequent cavities. Additionally, the upper surface of the active layer exhibited increased density.

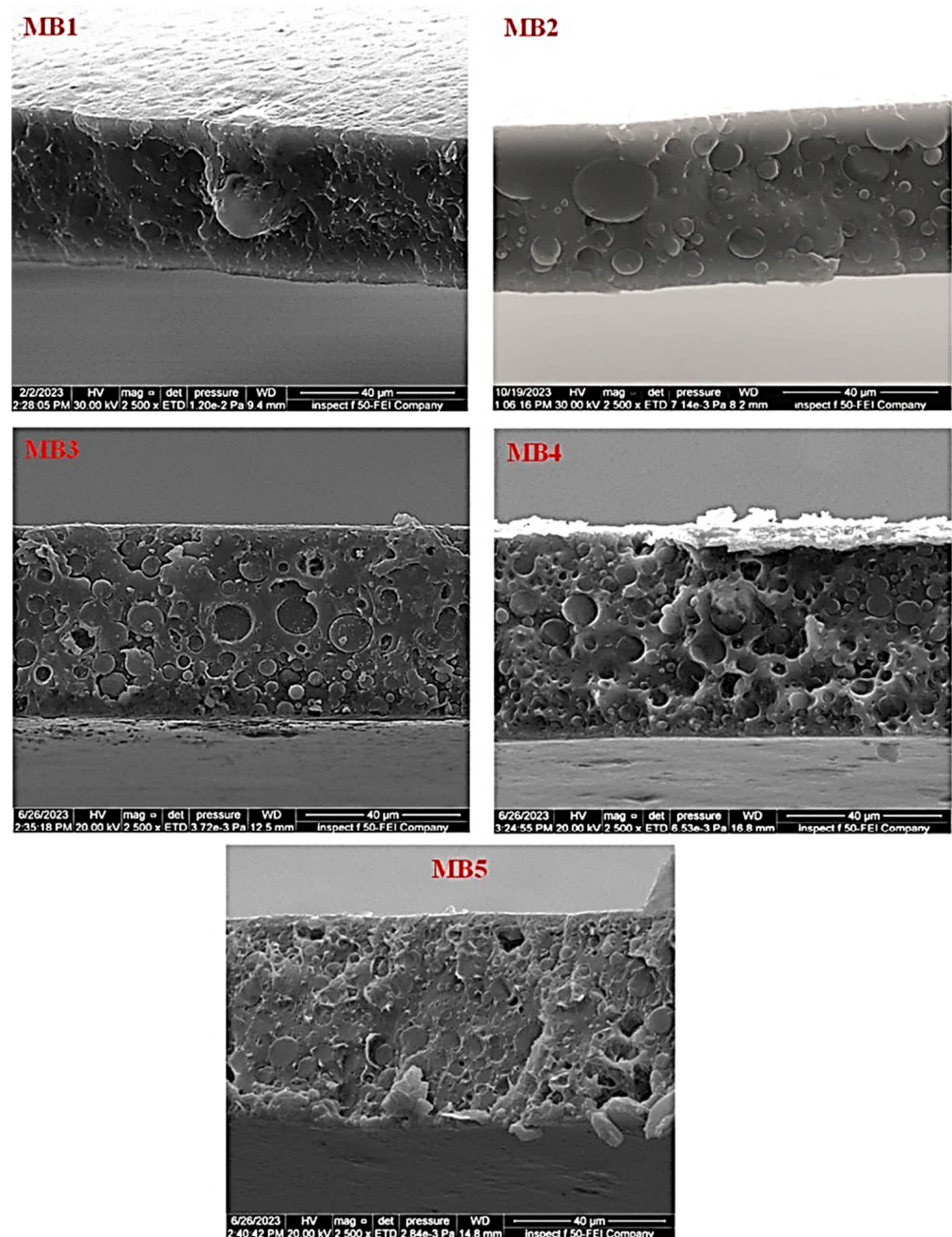


**Figure 5.** FESEM images of cross-sectional for the PLA/PBAT/BP membranes.

Similarly, an increase in BP-NP content led to a more compact arrangement on the upper surface, while the porous structure decreased, ultimately resulting in a denser structure, as illustrated in Figure 5 (MB5). In the absence of BP-NPs, as seen in Figure 4 (MB1), the intermolecular attraction between PLA/PBAT molecules intensified, leading to greater alignment and tightening of the pack support layer structure. During the phase inversion process, the membrane's pore density decreased due to the presence of tighter and denser structures that hindered the permeation of nonsolvent through the membrane's structure [43]. The incorporation of BP-NPs may reduce the intermolecular interaction

between PLA/PBAT molecules, resulting in decreased molecular orientation and a less organized pack support layer.

This effect is attributed to the hydrophilic nature of BP-NPs, which accelerates the rate of solvent–nonsolvent exchange (coagulation water bath) during the phase inversion process. This, in turn, leads to the formation of new pores [44]. The hydrophilic functional groups present in BP enable BP-NPs to migrate toward the membrane surface, thereby enhancing the membrane’s hydrophilicity [45].

### 3.1.3. Membrane Porosity, Mean Pore Size and Thickness

Critical variables directly influencing membrane performance include porosity and pore diameter, as they play a significant role in determining the efficiency of oil/water separation [46,47]. Figure 6A illustrates the porosity of PLA/PBAT and PLA/PBAT membranes with varying amounts of BP-NPs. The porosity of the PLA/PBAT membrane (MB1) increased from 50% to 58%, 61%, and 63% for the MB2, MB3, and MB4 membranes, respectively, due to the presence of BP-NPs in the casting solution. Consequently, MB4 exhibited a membrane structure with increased porosity. The hydrophilic BP-NPs in the dope solution accelerated the demixing process, resulting in an increased porosity [48]. However, as the BP-NP concentration was raised to 0.1 wt.% in the solution, the membrane porosity decreased to 57%. One possible explanation is that as the quantity of BP in the dope solution increased, BP molecules migrated from the porous structure and aggregated toward the membrane surface [49]. Nevertheless, the porosity of BP-incorporated membranes remained higher compared to the neat PLA/PBAT.

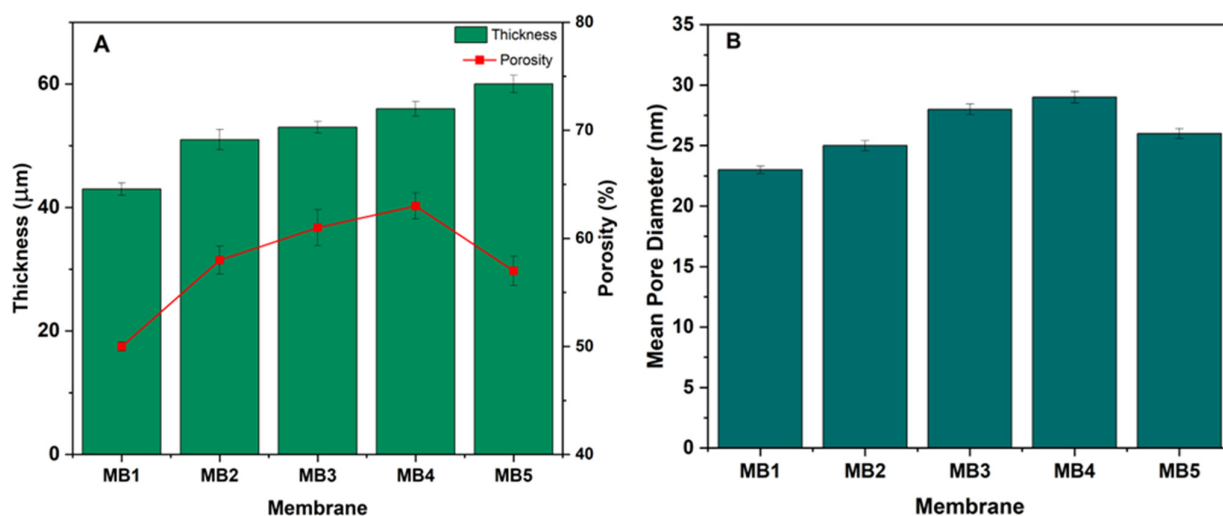


Figure 6. (A) PLA/PBAT/BP membrane thickness and porosity; (B) mean pore diameter.

Optimal membrane thickness typically falls within the range of 30 to 60 µm, although thinner membranes that maintain strength are also desirable [50]. Membrane thickness directly influences the solvent/nonsolvent inter-diffusion during the phase inversion process, as it is proportional to the polymer solution viscosity. Figure 6A displays the thickness of membranes fabricated using varying weight percentages of BP-NPs. The unmodified membrane had a thickness of 43 µm. Upon adding BP at a concentration of 0.025 wt.%, the thickness of MB2 and MB3 increased to 51 and 53 µm, respectively. Increased loading wt.% resulted in higher viscosity of the casting solution, leading to the formation of thicker layers (MB4 and MB5). The extended demixing process due to increased viscosity resulted in a longer precipitation process and thicker membrane formation [51,52]. Membrane thickness is a crucial factor affecting overall membrane performance.

Another vital characteristic impacting membrane performance is pore size [53]. Pore size measurements were significantly affected by the quantity of BP-NPs loaded within the PLA/PBAT membrane matrix (Figure 6B). BP-NPs substantially altered membrane pore

sizes compared to the unmodified membrane (PLA/PBAT). MB2 had an average pore size of 25 nm, while the PLA/PBAT membrane (MB1) had an average pore diameter of 23 nm. Increasing the BP amount further enlarged the average pore size, reaching a maximum of 29 nm at a loaded BP concentration of 0.05 wt.% (MB4).

The presence of hydrophilic BP-NPs increased the rate of solvent–nonsolvent interchange in the membrane dope solution, allowing a greater amount of water to permeate into the membrane structure [54]. However, when the BP-NPs content reached 0.01 wt.%, the membrane’s average pore size began to decrease significantly as BP-NPs started aggregating on the membrane surface [55,56].

#### 3.1.4. Hydrophilicity of the Membrane Surface

An important membrane feature is its hydrophilic surface, which can be assessed by measuring contact angles. Typically, a decrease in the contact angle of water indicates an increase in membrane hydrophilicity, whereas a larger contact angle suggests lower hydrophilicity [57]. Figure 7 displays the contact angles of water for both “PLA/PBAT” and “PLA/PBAT/BP” membranes fabricated using different concentrations of BP-NPs (0, 0.0125, 0.025, 0.05, and 0.1 wt.%). According to the data in Figure 7, the PLA/PBAT membrane exhibited the largest contact angle (73.71°), indicating the lowest hydrophilicity among the tested membranes. The incorporation of BP-NPs in the casting solution resulted in a reduction in contact angle (CA) values. Specifically, the CA values decreased from 73.71° to 50.8° and 41.3° for MB1, MB2, and MB3, respectively. The lowest contact angle (38.99°) was observed at a concentration of 0.05 wt.%. Therefore, it can be concluded that the inclusion of BP-NPs (up to 0.05 wt.%) as an additive positively affected the surface hydrophilic properties of the PLA/PBAT membrane. This finding can be attributed to the hydrophilic nature of BP-NPs. Previous studies have shown that BP-NPs migrate to the membrane’s surface layer during the fabrication process, resulting in increased hydrophilicity of the membrane’s surface layer. Similar findings have been reported in the academic literature [58,59]. Furthermore, the effect of BP-NPs on membrane contact angle (CA) values may be attributed to the reduction in interfacial energy and the high affinity between water and the hydrophilic nature of BP-NPs. Consequently, this leads to a reduction in CA values, indicating an increase in membrane hydrophilicity [60,61].

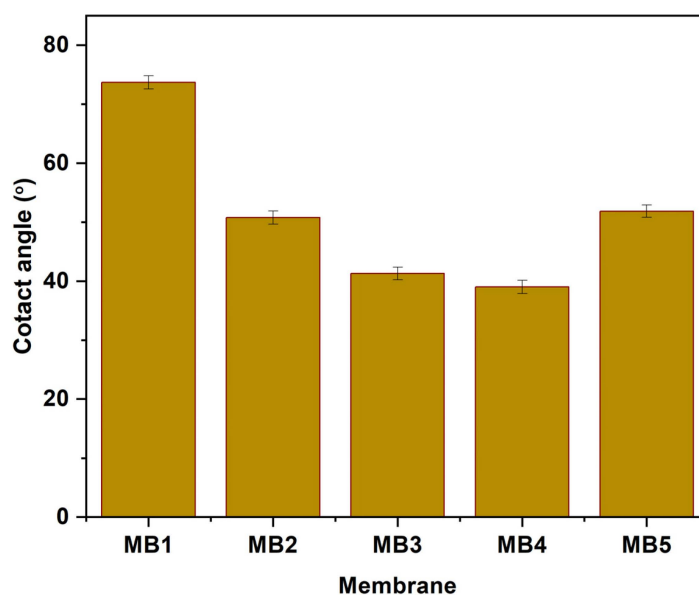


Figure 7. Contact angle of PLA/PBAT/BP membranes.

The water contact angle (CA) exhibited a slight increase when the added weight of the additive was raised to 0.1 wt.%, but it remained lower compared to the PLA/PBAT. Membranes altered with a weight percentage of 0.1% showed contact angles of approximately

51.88°. These observed outcomes are likely attributed to the aggregation of BP-NPs in a mesoporous structure, which reduced the effective surface area of the mesoporous material at higher concentrations of BP-NPs.

### 3.1.5. Tensile Strength, a Measure of Mechanical Properties

Mechanical characteristics of membrane strength represent an important measurement that indicates the long-term stability during industrial operation and its ability to withstand severe chemical cleaning. Figure 8 shows the findings of the study indicating “PLA/PBAT” tensile strength to be affected by the concentration of BP. The control (PLA/PBAT) membrane showed a value of 5.9 MPa, which was the lowest reported value compared to the other BP-modified membranes. Nevertheless, the membranes exhibited a significant increase in tensile strength, reaching an optimal value of 8.4 MPa, when including 0.05 wt.% BP-NPs in the dope solution. The enhancement may be due to the homogeneous dispersion of BP-NPs additives seen in the modified membrane, as well as the creation of a mechanically enhanced structure of membrane [62,63]. When the concentration of BP-NPs reaches 0.1 wt. %, the PLA/PBAT/BP tensile strength of is reduced due to the aggregation of the BP-NPs. This impedes the dispersion of stress and has the capacity to impact the crystalline structure, resulting in a reduction in tensile strength [64,65].

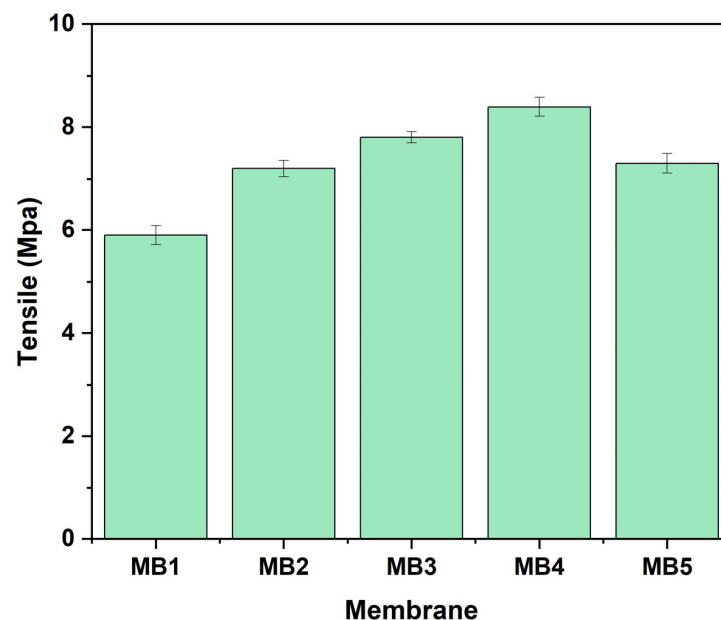


**Figure 8.** Tensile strength of PLA/PBAT/BP membrane.

## 3.2. Membranes Performance

### 3.2.1. PWF and the Oil Rejection

The effectiveness of a membrane depends on the interaction of many elements, such as pore size, porosity, and the membrane material hydrophilic properties [66,67]. The pure water flux and oil-in-water flux (at a pressure of 1.5 bar and an oil concentration of 100 ppm) were significantly impacted by the amount of BP-NP in the PLA/PBAT dope solution, as seen in Figure 9. The water permeates flux and oily wastewater permeate flux across the PLA/PBAT membrane were 62 and 28.6 L/m<sup>2</sup>h, respectively. Incorporating 0.05 wt.% of BP-NPs into the PLA/PBAT dope solution resulted in the maximum pure water permeability. Consequently, there was an increase in the pure water permeation to 105.31 L/m<sup>2</sup>h and 80 L/m<sup>2</sup>h for the permeate flux of oily wastewater. When the content of BP-NPs in the PLA/PBAT solution was increased, a rise in the porosity, average pore size, and hydrophilicity of the membrane was observed. This result can be used to explain the observed rise in PWF. It is important to note that the addition of more than 0.05 wt.% of BP-NPs led to a decrease in the permeate flux. The fabricated membranes at a concentration

of 0.1 wt. % BP-NPs demonstrated a flux of pure water (64.64 L/m<sup>2</sup>h), and the oil-in-water flux resulted in a permeate of 39.6 L/m<sup>2</sup>h. The agglomeration of BP-NPs on the PLA/PBAT membrane surface, at concentrations higher than 0.05 wt.%, resulted in decreased pore size, porosity, hydrophilicity; this agglomeration was assumed to be the cause of the reduction in permeate flux [68,69]. Hydrophilic membranes often exhibit a strong affinity for water. They are capable of forming hydrogen bonds with water and have very high surface energy values.

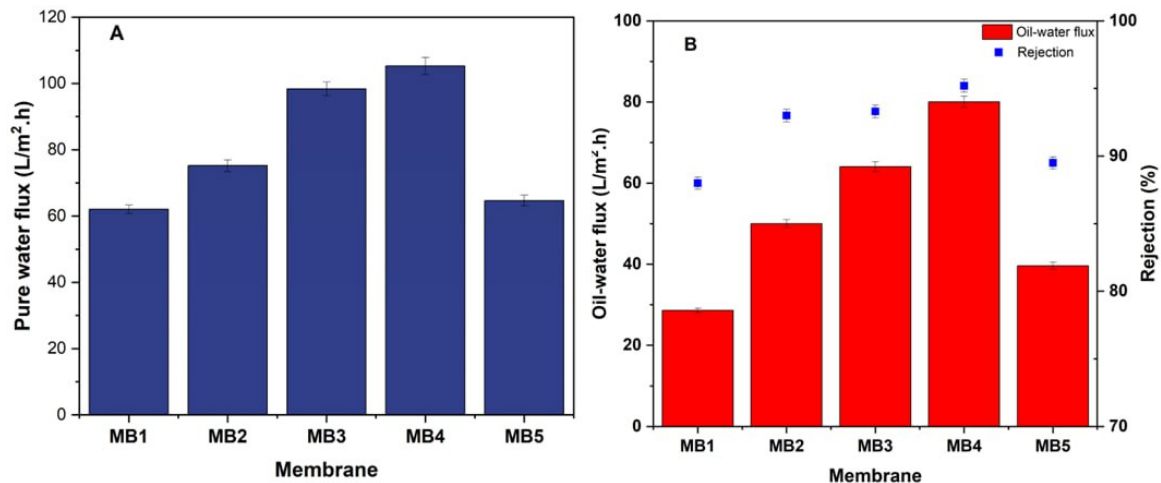


**Figure 9.** PLA/PBAT/BP membrane performance (A); pure water flux, (B); oily water flux and rejection (for 100 ppm oil at 1.5 bar).

Furthermore, the pure PLA/PBAT membranes have shown a retention rate of 88% for oil/water emulsions with a concentration of 100 ppm oil and a transmembrane pressure of 1.5 bar, as shown in Figure 9B. Simultaneously, the efficiency of rejecting the oil/water emulsion notably increased to about 93%, 93.3%, and 95.2% by including 0.0125, 0.025, and 0.05 wt.% BP-NPs into the PLA/PBAT dope solution, respectively. This behavior may be attributed to the presence of hydrophilic BP-NPs, which enhance the surface membrane hydrophilicity [70]. Water is easily trapped on the membrane surface, forming a layer of water. The hydrophobic nature of oil prevents it from adsorbing onto the membrane surface, because of the presence of the water layer. The improvement of surface structures in oil-in-water separation has led to the formation of oleophobic surfaces with less oil adhesion [71,72]. In addition, when the content of BP-NPs was raised to 0.1 wt.%, the (oil/water) emulsion rejection decreased to 89.5%. The reduction in the oil rejection may be attributed to a high amount of aggregation of BP-NPs. This leads to the intermittent creation of flaws through the membrane manufacturing process, which can negatively affect the percentage of membrane rejection [73]. Furthermore, researchers have also reported similar findings, indicating that raising the concentration of nanofillers causes the formation of agglomerates and a decrease in dispersion within the polymer matrix. This phenomenon may explain the observed reduction in rejection [74,75].

### 3.2.2. Effect of Operating Pressure on Membrane Performance

Optimizing operating conditions has a significant impact on the performance effectiveness of manufactured membranes. Herein, the effects of changing the transmembrane pressure range (1.5, 2.5, and 3.5 bar) on the oil rejection and permeate flux of the PLA/PBAT membrane (MB1) and the best PLA/PBAT/BP membrane (MB4) were examined (Figure 10).

Figure 10A demonstrates the impact of transmembrane pressure on the flux of oil/water through a permeable membrane under steady conditions. By raising the operating pressure between 1.5 and 3.5 bar, it is seen that the flux of oily wastewater also increases. Specifically, for MB1, the flux increases from 28.6 L/m<sup>2</sup>h to 75.7 L/m<sup>2</sup>h, and for MB4, the flux increases from 80 L/m<sup>2</sup>h to 135 L/m<sup>2</sup>h. It was found that the fluxes increased as the pressure

increased. Flux is directly related to the net pressure difference across the membrane in the solution and diffusion model. An increase in the membrane pressure may cause some deformation in polymeric chains as well as in pores' dimensions. More permeate passes through the voids as a result of chain movement. However, over time, membrane flux decreases because oil droplets that manage to pass through the surface of the membrane later block the pores available on the surface and throughout the cross-section. Moreover, the overall flux of the membrane decreases as a result of the formation of a resistant layer on the surface of the membrane. T. Mohammadi and A. Esmaelifar studied the effect of operating pressure on the membrane permeate flux and found that increasing pressure increases permeation flux but higher pressures cause the cake layer formed on the membrane surface to compress, accelerating membrane fouling. Thus, at optimum pressure, permeation flux is high and the tendency of cake layer formation is low. According to Darcy's Law, as pressure increases, while other operating parameters remain constant, permeation flux increases. Fouling experiments were carried out at different pressures. Investigations of permeation flux as a function of time at different pressures show that the trend in variations at all pressures is almost the same. In all cases, after a definite time, permeation flux reaches a constant value depending on the operating pressure. Flux decline at different pressures can be compared. The results showed that, at higher pressures, flux decline is greater. According to the results, at all pressure levels, after about 60 min, flux reaches a constant value. This is because, after this time, the cake layer reaches equilibrium and its growth ceases. Therefore, the cake layer resistance and subsequent permeation flux remain constant. Membrane resistance ( $R_m$ ) does not change with pressure whereas fouling resistance ( $R_f$ ) increases as pressure increases. Until a pressure of  $3 \times 10^5$  Pa (3 bar),  $R_f$  increases; however, after that, it does not change considerably and remains nearly constant. Thus, a pressure of  $3 \times 10^5$  Pa (3 bar) is the lowest operating pressure because, at higher pressures, permeation flux increases as pressure increases but  $R_f$  does not change any more [76,77]. Additionally, increasing the transmembrane pressure enhances the flux of the permeate by raising the shear stress on the membrane surface. This accelerates the removal of deposited solutes that cause a decline in flux [78].

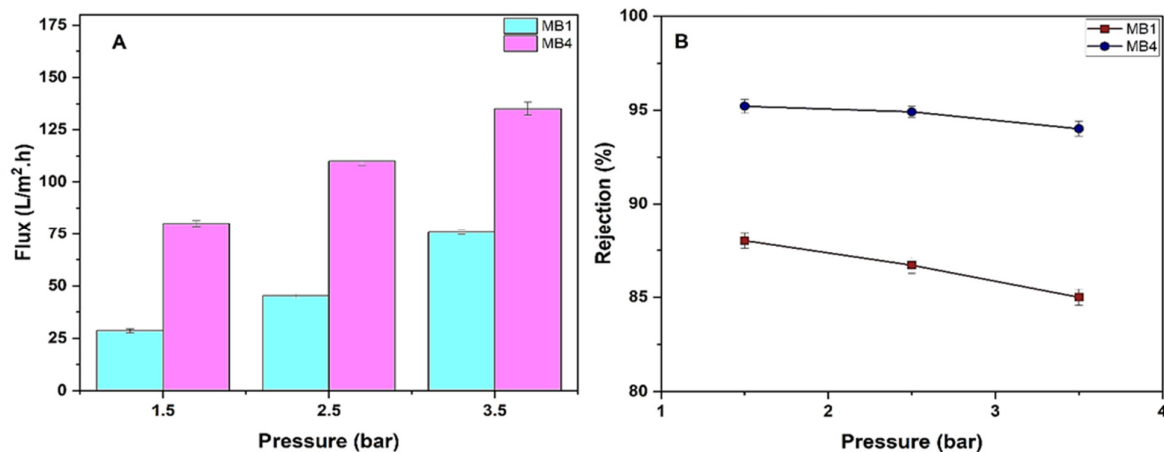


**Figure 10.** PLA/PBAT/BP membrane performance. (A) Flux of permeate; (B) rejection of oil (for 100 ppm oil at 1.5, 2.5, and 3.5 bar).

The oil rejection of MB1 was 88% at 1.5 bar and decreased to 85% at 3.5 bar. However, when utilizing MB4, the oil rejection was 95.2% at 1.5 bar and 94% at 3.5 bar, as seen in Figure 10B. Similar findings have also been observed in other studies [79,80].

### 3.2.3. Influence of Feed Concentration on the Membrane Performance

Filtering experiments were carried out to assess the effectiveness of the manufactured membrane using feeds with varying oil/water emulsion concentrations (100, 200, and

300 ppm) at a pressure of 1.5 bar. Figure 11 illustrates the flux of three different feed solutions utilizing oil/water emulsions. The findings revealed that a concentration increase in the feed results in a reduction in the flux of the permeate of the oil/water emulsion. The findings (Figure 11A) demonstrated that the rate of permeate flux decreased as the oil content increased. The permeate of MB1 reduced from 28.6 to 11.2 L/m<sup>2</sup>h, and for MB4, it reduced from 80 L/m<sup>2</sup>h to 41 L/m<sup>2</sup>h as the oil concentration increased from 100 to 300 ppm. The oil molecule accumulation on the membrane caused a drop in permeation fluxes. This occurred due to blockage and/or reduction in the membrane pores size, leading to a decrease in the membrane's permeation flux [81,82].

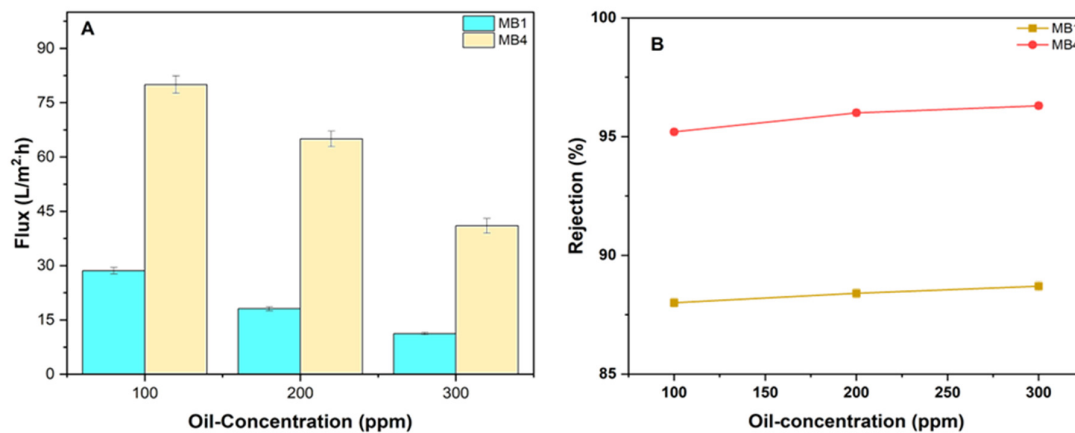
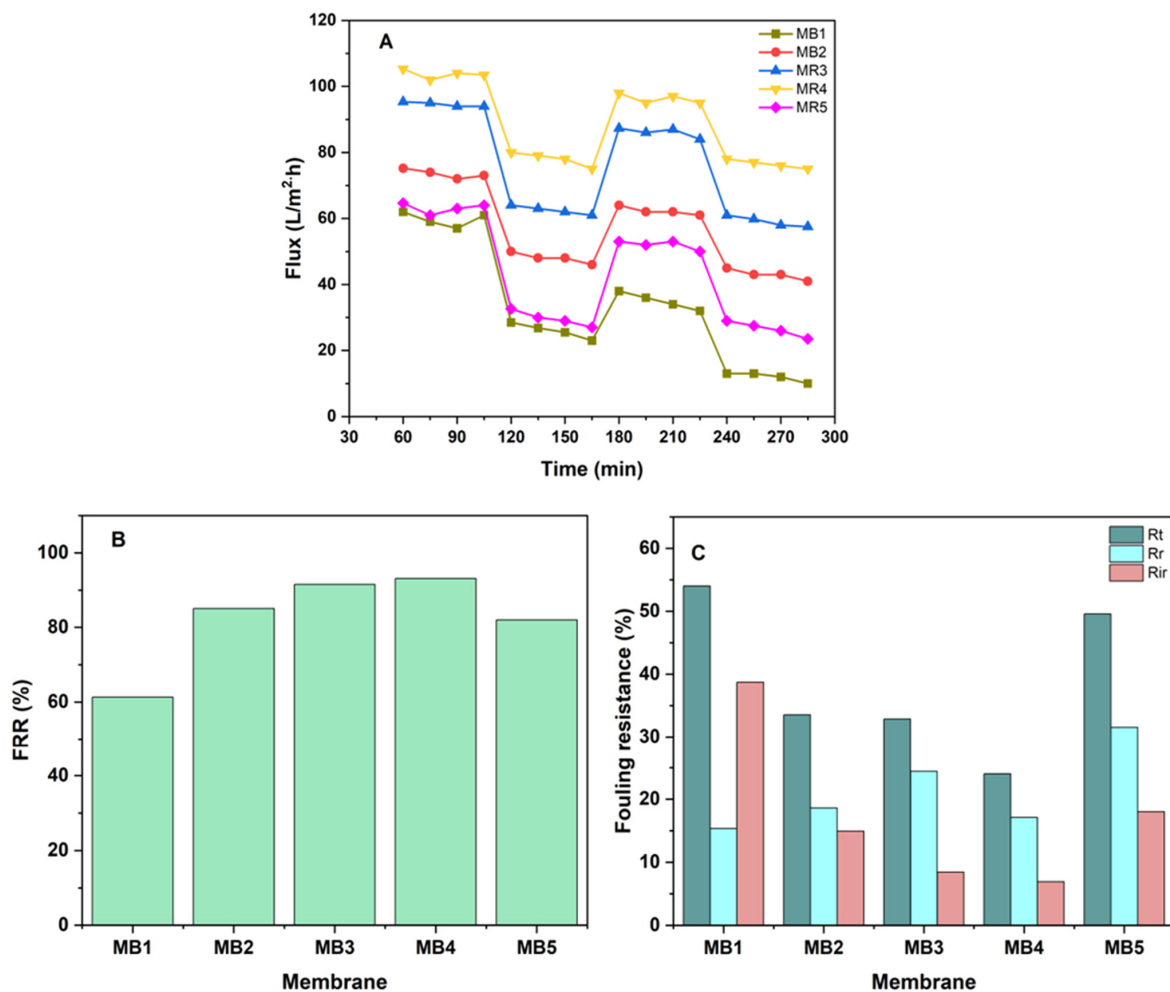


**Figure 11.** PLA/PBAT/BP membrane performance. (A) Flux of permeate; (B) rejection of oil for (100, 200, and 300 ppm oil at 1.5 bar).

Furthermore, examinations were carried out to find out the impact of increasing the concentration of feed on the membrane's rejection. The impact of various oil/water feed concentrations is seen in Figure 11B. Increasing the concentration of the oil/water emulsion results in an increase in membrane rejection. The rejection of oil by the PLA/PBAT membrane (MB1) was 88% at an oil concentration of 100 ppm, whereas the modified membrane (MB3) had an oil rejection of 95.2%. At an oil concentration of 300 ppm, the oil rejection increased to 88.7% for MB1 and 96.3% for MB3. The presence of oil molecules on the membrane surface may result in the formation of a compact thin layer, thus increasing the overall rejection rate [83,84].

#### 3.2.4. Flux Recovery and Antifouling Efficacy Analysis

One of the most typical problems related to membrane technologies is membrane fouling, which may adversely impact the performance in terms of both the quality and quantity of the membrane. Attributes that a good membrane needs to have include a high rate of flux, great fouling resistance, and a satisfactory degree of separation efficiency that can be maintained for a long time [85]. Enhancing the hydrophilicity of membranes has long been recognized as an effective and suitable approach to addressing fouling problems. Since the development of membranes, this problem has attracted a significant amount of attention and interest [86]. Antifouling experiments were performed on both the pure and BP-modified membranes for two cycles of extended operation, which were then followed by a washing process (Figure 12A). The permeability of membranes remained mostly stable throughout operation with pure water. After one hour of operation, the flux across each membrane gradually decreased when the feed was replaced with oil/water emulsions. This is due to the oil accumulation on both the surface and inside the structure of the membrane. Then, both membranes underwent a 30 min cleaning process using deionized water in order to reinstate its initial flux. A similar process was carried out by Yang et al., who obtained similar outcomes with this type of behavior [87].



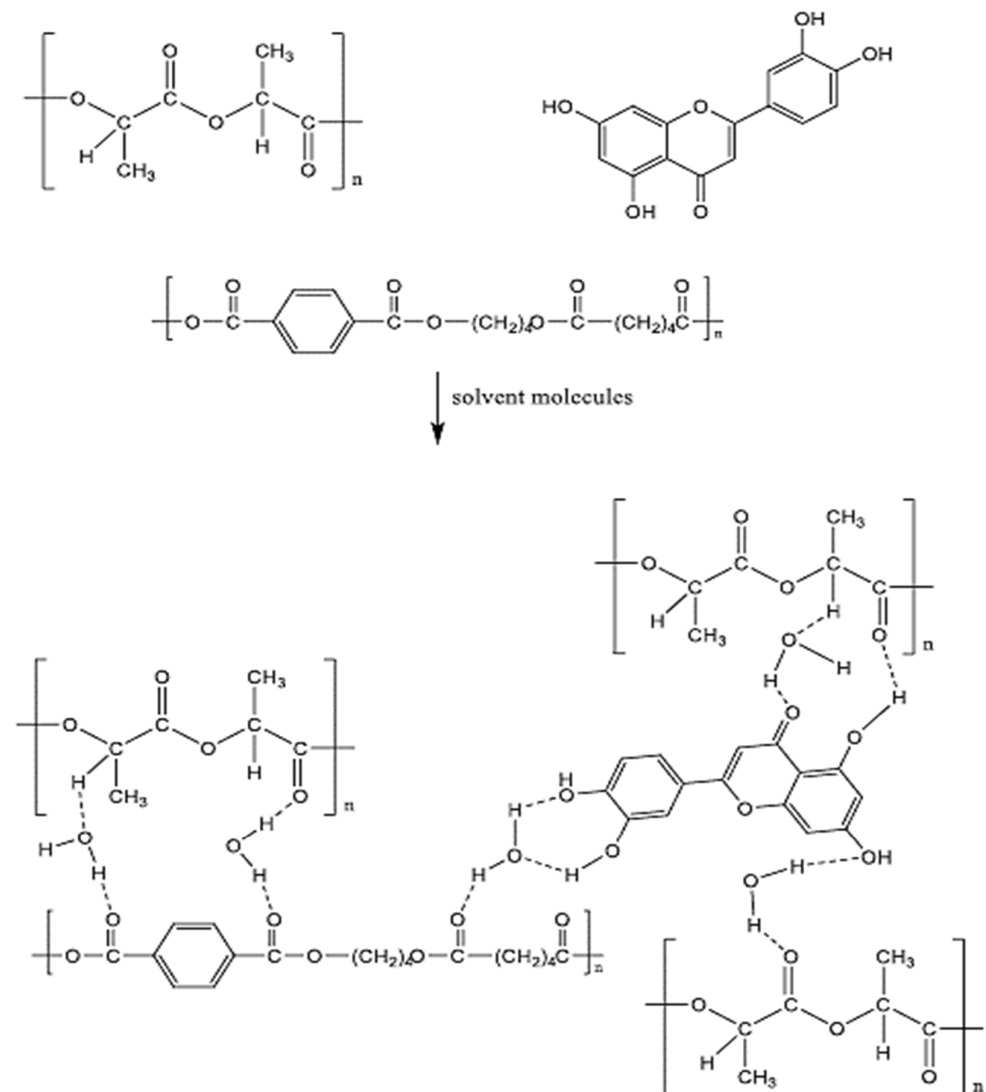
**Figure 12.** (A) Membrane flux before and after cleaning; (B) FRR; (C) Rt, Rr and Rir of PLA/PBAT/BP membrane at 100 ppm oil and 1.5 bar of pressure.

Figure 12B,C show the end results, which included determining the total fouling (Rt), irreversible fouling (Rir), and reversible fouling (Rr) in addition to the ratio of flux recovery (FRR). Figure 12B shows that the FRR of the PLA/PBAT membrane was 61%, whereas the PLA/PBAT/BP membranes achieved FRRs of 85%, 91%, 93%, and 81% for MB2, MB3, MB4, and MB5, respectively. The primary cause of membrane fouling is the adsorption of foulants into the surface of the membrane and their subsequent entrapment inside the pores. The Rr values found in all PLA/PBAT/BP membranes were higher than those of the pure PLA/PBAT membrane. In contrast, the Rir values exhibited a decrease compared to the pure PLA/PBAT membrane. The PLA/PBAT membranes exhibited Rt, Rr, and Rir values of 54%, 15%, and 38%, respectively. The PLA/PBAT/BP membrane exhibited percentages of 49%, 31%, and 18% for MB5, respectively, as seen in Figure 12C. The reduction in Rir and increase in Rr indicated that the oil particles that were accumulating on the membrane's surface became easy to removed. Possible explanations include enhanced hydrophilicity and a homogeneous pore structure. Based on the obtained results, it appears that the modification of BP-NPs has the potential to enhance the effectiveness of antifouling for a PLA/PBAT membrane. Findings that were similar to this trend were also found in other studies [88,89].

### 3.3. Proposed Interaction Mechanisms

Research has shown that the addition of BP-NPs may enhance the performance and antifouling properties of modified membranes. The increased attraction between the BP

nanoparticles and the PLA/PBAT series may explain the improved surface properties of the modified membranes. Based on the results, the PLA/PBAT and BP-NP membranes undergo the following interaction processes, which modify their interactions with water molecules, as shown in Figure 13. The inclusion of hydrophilic functional groups, which are flexible, may explain why the BP-NP chain and the PLA/PBAT chain are more compatible; this, in turn, causes the surface characteristics of PLA/PBAT MMMs to be changeable. This is a direct representation of the nature of the interactions between water molecules and the surface of the membrane. The presence of these functional groups facilitates the formation of hydrogen bonds between water molecules. As a consequence, a wetting layer is formed on the surface of the membrane, leading to substantial enhancement of both the wettability and permeability of the membrane. Consequently, the overall efficiency of the system is also much improved. Electronegative elements, such as oxygen, enhance the likelihood of hydrogen bonds being formed. Moreover, the strong electronegativity of oxygen causes most of its electron density to be pulled away from its covalent link with hydrogen. The interaction between hydrogen and oxygen atoms results in the creation of a sealed enclosure that can hold water, thereby causing an elevation in the hydrophilic nature of MMM.



**Figure 13.** Proposed interaction mechanisms between PLA/PBAT/BP membrane components.

### 3.4. Comparison in Relation to Other Literary Works

Table 2 shows a comparison of various membrane performances listed in the literature with that of the PLA/PBAT/BP membranes used in this investigation for the ultrafiltration application. The comparison took into account many properties of the membranes, such as the kind of additive, type of oil, oil concentration, porosity, contact angle (CA), flux, FRR%, and removal (%). Considering the efficiency of oil removal and the pure water flux compared to various membranes discussed in the scientific literature, the PLA/PBAT/BP membrane demonstrates good performance with a considerable proportion of removal.

**Table 2.** Performance comparison of PLA/PBAT/BP membrane with different kinds of polymers that have been enhanced by additives to remove oil from water.

Membrane	Nanoparticle Type	Oil Type	Oil Conc.	Porosity	Contact Angle (°)	Permeation (L/m <sup>2</sup> h)	FRR (%)	Removal (%)	Ref.
CSPNMs	Corn straw	<i>n</i> -hexane, toluene and diesel	4,2,4/120 mL (oil/water)	/	/	660	/	>99.60	[23]
MCA-MCS- TiO <sub>2</sub>	TiO <sub>2</sub>	cyclohexane	2/200 mL (oil/water)	/	13.7	109.5	/	99.4	[90]
PVC/MWCNT-g-GO	MWCNT-g-GO	oil	/	81.4	13.9	254	/	88.9	[91]
PVC-TiO <sub>2</sub>	TiO <sub>2</sub>	Oil and grease	40.14 mg/L	79.5	62.5	116	89.9	96.3	[92]
EGCG-PVDF	EGCG	diesel oil	1 g/L	/	41	735	98.1%	95.5	[93]
PVC/GO-ZnO	GO-ZnO	Industrial vegetable oil	1000 mg/L	increased	67	1526.71	35.8	99.55	[94]
FP@SA/CaCO <sub>3</sub>	CaCO <sub>3</sub>	Different oil	20/20 mL (oil/water)	/	0	400	/	99.2	[95]
PPSU/TiO <sub>2</sub>	TiO <sub>2</sub>	oil	/	/	64	54.53	82.5	92.95	[96]
PVC/AAm-g-bentonite	AAm-g-bentonite	Crude oil	400 mg/L	71.22	49.1	293.14	82.1	93.2	[97]
PLA	TiO <sub>2</sub>	Different oil	1/1 (v/v) (oil/water)	/	0	950	/	>99	[14]
PLA, PPC, PHB, PBS	SiO <sub>2</sub>	Oil and grease	17.12 mg/l	/	/	/	/	>98	[98]
PLA	SiO <sub>2</sub>	Different oil	10/90 mL (oil/water)	/	0	1142-1485	>90	>99	[99]
PLA/PBAT/BP	BP	Diesel oil	300 ppm	68.1	38.99	105.3	93	96.5	This work

## 4. Conclusions

In this research, phase inversion was used to synthesize PLA/PBAT and PLA/PBAT/BP membranes for the treatment of oily wastewater. BP-NPs were utilized to solve the fouling and wettability issues with PLA/PBAT membranes due to their high hydrophilic features. The incorporation of BP-NPs in the PLA/PBAT membrane matrix was confirmed using the FTIR test. The FESEM cross-section and surface pictures revealed significant changes in the membrane structure upon the addition of BP-NPs, which resulted in the enhancement of the porosity and pore size of the modified membranes. The tensile strength of the nanocomposite membranes was greater in addition to their enhanced porosity. By raising the BP-NP content to 0.05 wt.%, the nanocomposite membranes' contact angle was dramatically reduced, leading to a notable improvement in pure water flux. The lowest (62 L/m<sup>2</sup>h) and highest (105.3 L/m<sup>2</sup>h) pure water flux corresponded to the unmodified and modified membranes with 0.05 wt.% of BP-NPs, respectively. Modified membranes (MB4) also showed the highest oil removal efficiency (96.3%) at 300 ppm. Hydrophilicity is the most important characteristic in fouling and FRR. As the membrane surface becomes more hydrophilic, the affinity of water molecules to interact with the functional groups of membranes rises, preventing organic foulant adsorption. A higher FRR (93%) was obtained for the modified MB4 membrane compared to FRR obtained for the unmodified MB1 membrane (61%). It was demonstrated that green membranes with various morphologies could be produced and used in various oily wastewater treatment processes. Nonetheless,

a great deal of work still has to be carried out to create fully sustainable membranes that function at least as well as conventional membranes in real applications.

**Author Contributions:** Conceptualization, Q.F.A. and K.T.R.; methodology, Q.F.A., M.Y.G., I.T.I. and K.T.R.; software, Z.M.S. and I.H. validation, Q.F.A., K.T.R., M.Y.G. and Z.M.S.; formal analysis, I.T.I. and K.T.R.; investigation, Q.F.A., K.T.R. and A.A.A.; writing—original draft preparation, Q.F.A., M.Y.G., K.T.R. and A.A.A.; writing—review and editing, Q.F.A., A.A.A. and I.T.I.; supervision, Q.F.A. and K.T.R. All authors have read and agreed to the published version of the manuscript.

**Funding:** This research received no external funding.

**Data Availability Statement:** Data is contained within the article.

**Conflicts of Interest:** The authors declare no conflict of interest.

## References

1. Gohari, R.J.; Korminouri, F.; Lau, W.; Ismail, A.; Matsuura, T.; Chowdhury, M.; Halakoo, E.; Gohari, M.J. A novel super-hydrophilic PSf/HAO nanocomposite ultrafiltration membrane for efficient separation of oil/water emulsion. *Sep. Purif. Technol.* **2015**, *150*, 13–20. [[CrossRef](#)]
2. Ahmad, N.A.; Goh, P.S.; Karim, Z.A.; Ismail, A.F. Thin film composite membrane for oily waste water treatment: Recent advances and challenges. *Membranes* **2018**, *8*, 86. [[CrossRef](#)] [[PubMed](#)]
3. Junaidi, N.F.D.; Othman, N.H.; Shahrudin, M.Z.; Alias, N.H.; Marpani, F.; Lau, W.J.; Ismail, A.F. Fabrication and characterization of graphene oxide–polyethersulfone (GO–PES) composite flat sheet and hollow fiber membranes for oil–water separation. *J. Chem. Technol. Biotechnol.* **2020**, *95*, 1308–1320. [[CrossRef](#)]
4. Ikhsan, S.N.W.; Yusof, N.; Aziz, F.; Misdan, N.; Ismail, A.F.; Lau, W.-J.; Jaafar, J.; Salleh, W.N.W.; Hairom, N.H.H. Efficient separation of oily wastewater using polyethersulfone mixed matrix membrane incorporated with halloysite nanotube-hydrous ferric oxide nanoparticle. *Sep. Purif. Technol.* **2018**, *199*, 161–169. [[CrossRef](#)]
5. Ghadhban, M.Y.; Majdi, H.S.; Rashid, K.T.; Alsahy, Q.F.; Lakshmi, D.S.; Salih, I.K.; Figoli, A. Removal of dye from a leather tanning factory by flat-sheet blend ultrafiltration (UF) membrane. *Membranes* **2020**, *10*, 47. [[CrossRef](#)] [[PubMed](#)]
6. Zhu, X.; Tu, W.; Wee, K.-H.; Bai, R. Effective and low fouling oil/water separation by a novel hollow fiber membrane with both hydrophilic and oleophobic surface properties. *J. Membr. Sci.* **2014**, *466*, 36–44. [[CrossRef](#)]
7. Ghadhban, M.Y.; Rashid, K.T.; AbdulRazak, A.A.; Alsahy, Q.F. Recent progress and future directions of membranes green polymers for oily wastewater treatment. *Water Sci. Technol.* **2023**, *87*, 57–82. [[CrossRef](#)] [[PubMed](#)]
8. Chai, P.; Choy, P.; Teoh, W.; Mahmoudi, E.; Ang, W. Graphene oxide based mixed matrix membrane in the presence of eco-friendly natural additive gum Arabic. *J. Environ. Chem. Eng.* **2021**, *9*, 105638. [[CrossRef](#)]
9. Ye, B.; Jia, C.; Li, Z.; Li, L.; Zhao, Q.; Wang, J.; Wu, H. Solution-blow spun PLA/SiO<sub>2</sub> nanofiber membranes toward high efficiency oil/water separation. *J. Appl. Polym. Sci.* **2020**, *137*, 1–9. [[CrossRef](#)]
10. Raja, R.I.; Rashid, K.T.; Toma, M.; AbdulRazak, A.A.; Shehab, M.A.; Hernadi, K. A Novel Polyethersulfone/Chamomile (PES/Chm) Mixed Matrix Membranes for Wastewater Treatment Applications. *J. Saudi Chem. Soc.* **2024**, *28*, 101805. [[CrossRef](#)]
11. Deng, Y.; Zhang, G.; Bai, R.; Shen, S.; Zhou, X.; Wyman, I. Fabrication of superhydrophilic and underwater superoleophobic membranes via an in situ crosslinking blend strategy for highly efficient oil/water emulsion separation. *J. Membr. Sci.* **2019**, *569*, 60–70. [[CrossRef](#)]
12. Goh, P.S.; Ng, B.C.; Lau, W.J.; Ismail, A. Inorganic nanomaterials in polymeric ultrafiltration membranes for water treatment. *Sep. Purif. Rev.* **2015**, *44*, 216–249. [[CrossRef](#)]
13. Geleta, T.A.; Maggay, I.V.; Chang, Y.; Venault, A. Recent Advances on the Fabrication of Antifouling Phase-Inversion Membranes by Physical Blending Modification Method. *Membranes* **2023**, *13*, 58. [[CrossRef](#)] [[PubMed](#)]
14. Xiong, Z.; Lin, H.; Zhong, Y.; Qin, Y.; Li, T.; Liu, F. Robust superhydrophilic polylactide (PLA) membranes with a TiO<sub>2</sub> nano-particle inlaid surface for oil/water separation. *J. Mater. Chem. A* **2017**, *5*, 6538–6545. [[CrossRef](#)]
15. Ismail, N.H.; Salleh, W.N.W.; Awang, N.A.; Ahmad, S.Z.N.; Rosman, N.; Sazali, N.; Ismail, A.F. PVDF/HMO ultrafiltration membrane for efficient oil/water separation. *Chem. Eng. Commun.* **2021**, *208*, 463–473. [[CrossRef](#)]
16. Jiang, S.; Ladewig, B.P. Green synthesis of polymeric membranes: Recent advances and future prospects. *Curr. Opin. Green Sustain. Chem.* **2020**, *21*, 1–8. [[CrossRef](#)]
17. Ali, A.M.; Rashid, K.T.; Yahya, A.A.; Majdi, H.S.; Salih, I.K.; Yusoh, K.; Alsahy, Q.F.; AbdulRazak, A.A.; Figoli, A. Fabrication of gum arabic-graphene (Gga) modified polyphenylsulfone (ppsu) mixed matrix membranes: A systematic evaluation study for ultrafiltration (uf) applications. *Membranes* **2021**, *11*, 542. [[CrossRef](#)] [[PubMed](#)]
18. Morales-Jiménez, M.; Palacio, D.A.; Palencia, M.; Meléndrez, M.F.; Rivas, B.L. Bio-Based Polymeric Membranes: Development and Environmental Applications. *Membranes* **2023**, *13*, 625. [[CrossRef](#)] [[PubMed](#)]
19. Singh, H.; Desimone, M.F.; Pandya, S.; Jasani, S.; George, N.; Adnan, M.; Aldarhami, A.; Bazaid, A.S.; Alderhami, S.A. Revisiting the Green Synthesis of Nanoparticles: Uncovering Influences of Plant Extracts as Reducing Agents for Enhanced Synthesis Efficiency and Its Biomedical Applications. *Int. J. Nanomed.* **2023**, *18*, 4727–4750. [[CrossRef](#)]

20. Castro, R.S.D.; Caetano, L.; Ferreira, G.; Padilha, P.M.; Saeki, M.J.; Zara, L.F.; Martines, M.A.U.; Castro, G.R. Banana Peel applied to the solid phase extraction of copper and lead from river water: Preconcentration of metal ions with a fruit waste. *Ind. Eng. Chem. Res.* **2011**, *50*, 3446–3451. [[CrossRef](#)]
21. Chen, M.; Zhu, L.; Dong, Y.; Li, L.; Liu, J. Waste-to-Resource Strategy to Fabricate Highly Porous Whisker-Structured Mullite Ceramic Membrane for Simulated Oil-in-Water Emulsion Wastewater Treatment. *ACS Sustain. Chem. Eng.* **2016**, *4*, 2098–2106. [[CrossRef](#)]
22. Zang, D.; Zhang, M.; Liu, F.; Wang, C. Superhydrophobic/superoleophilic corn straw fibers as effective oil sorbents for the recovery of spilled oil. *J. Chem. Technol. Biotechnol.* **2016**, *91*, 2449–2456. [[CrossRef](#)]
23. Yu, Q.; Zhang, W.; Zhao, X.; Cao, G.; Liu, F.; Di, X.; Yang, H.; Wang, Y.; Wang, C. A simple, green method to fabricate composite membranes for effective oil-in-water emulsion separation. *Polymers* **2018**, *10*, 323. [[CrossRef](#)]
24. Li, J.; Li, D.; Yang, Y.; Li, J.; Zha, F.; Lei, Z. A prewetting induced underwater superoleophobic or underoil (super) hydrophobic waste potato residue-coated mesh for selective efficient oil/water separation. *Green Chem.* **2016**, *18*, 541–549. [[CrossRef](#)]
25. Abdulfatai, J.; Saka, A.A.; Afolabi, A.S.; Micheal, O. Development of adsorbent from banana peel for wastewater treatment. *Appl. Mech. Mater.* **2013**, *248*, 310–315. [[CrossRef](#)]
26. Raturi, P.; Panwar, V.; Khanduri, P. Formation of ionic polymer membrane by using banana peel. *Mater. Today Proc.* **2021**, *44*, 1898–1902. [[CrossRef](#)]
27. Ferreira, E.d.S.; Paranhos, S.B.; da Paz, S.P.A.; Canelas, C.A.d.A.; Nascimento, L.A.S.D.; Passos, M.F.; da Silva, A.C.R.; Monteiro, S.N.; Paula, M.V.d.S.; Candido, V.S. Synthesis and Characterization of Natural Polymeric Membranes Composed of Chitosan, Green Banana Peel Extract and Andiroba Oil. *Polymers* **2022**, *14*, 1105. [[CrossRef](#)] [[PubMed](#)]
28. Dmitrieva, E.S.; Anokhina, T.S.; Novitsky, E.G.; Volkov, V.V.; Borisov, I.L.; Volkov, A.V. Polymeric Membranes for Oil-Water Separation: A Review. *Polymers* **2022**, *14*, 980. [[CrossRef](#)] [[PubMed](#)]
29. Nayab, S.S.; Abbas, M.A.; Mushtaq, S.; Khan Niazi, B.; Batool, M.; Shehnaz, G.; Ahmad, N.; Ahmad, N.M. Anti-foulant ultrafiltration polymer composite membranes incorporated with composite activated carbon/chitosan and activated carbon/thiolated chitosan with enhanced hydrophilicity. *Membranes* **2021**, *11*, 827. [[CrossRef](#)]
30. Fan, S.; Aghajani, M.; Wang, M.; Martinez, J.; Ding, Y. Patterning flat-sheet Poly(vinylidene fluoride) membrane using templated thermally induced phase separation. *J. Membr. Sci.* **2020**, *616*, 118627. [[CrossRef](#)]
31. Han, L.; Shen, L.; Lin, H.; Cheng, T.; Wen, J.; Zeng, Q.; Xu, Y.; Li, R.; Zhang, M.; Hong, H.; et al. Three dimension-printed membrane for ultrafast oil/water separation as driven by gravitation. *Nano Energy* **2023**, *111*, 108351. [[CrossRef](#)]
32. Maccaferri, E.; Cocchi, D.; Mazzocchetti, L.; Benelli, T.; Brugo, T.M.; Giorgini, L.; Zucchelli, A. How Nanofibers Carry the Load: Toward a Universal and Reliable Approach for Tensile Testing of Polymeric Nanofibrous Membranes. *Macromol. Mater. Eng.* **2021**, *306*, 2100183. [[CrossRef](#)]
33. Jafarian, H.; Firouzjaei, M.D.; Aktij, S.A.; Aghaei, A.; Khomami, M.P.; Elliott, M.; Wujcik, E.K.; Sadrzadeh, M.; Rahimpour, A. Synthesis of heterogeneous metal organic Framework-Graphene oxide nanocomposite membranes for water treatment. *Chem. Eng. J.* **2023**, *455*, 140851. [[CrossRef](#)]
34. Zhang, X.; Wei, C.; Ma, S.; Zhang, C.; Li, Y.; Chen, D.; Xu, Z.; Huang, X. Janus poly(vinylidene fluoride)-graft-(TiO<sub>2</sub> nanoparticles and PFDS) membranes with loose architecture and asymmetric wettability for efficient switchable separation of surfactant-stabilized oil/water emulsions. *J. Membr. Sci.* **2021**, *640*, 119837. [[CrossRef](#)]
35. Zhu, X.; Yu, Z.; Zeng, H.; Feng, X.; Liu, Y.; Cao, K.; Li, X.; Long, R. Using a simple method to prepare UiO-66-NH<sub>2</sub>/chitosan composite membranes for oil–water separation. *J. Appl. Polym. Sci.* **2021**, *138*, 50765. [[CrossRef](#)]
36. Mehranbod, N.; Khorram, M.; Azizi, S.; Khakinezhad, N. Modification and superhydrophilization of electrospun polyvinylidene fluoride membrane using graphene oxide-chitosan nanostructure and performance evaluation in oil/water separation. *J. Environ. Chem. Eng.* **2021**, *9*, 106245. [[CrossRef](#)]
37. Shami, R.; Sabir, A.; Iqbal, S.S.; Gull, N.; Zohra, R.; Khan, S.M. Synergistic effect of GO/ZnO loading on the performance of cellulose acetate/chitosan blended reverse osmosis membranes for NOM rejection. *Heliyon* **2023**, *9*, e13736. [[CrossRef](#)] [[PubMed](#)]
38. Kamel, N.A.; El-Messieh, S.L.A.; Saleh, N.M. Chitosan/banana peel powder nanocomposites for wound dressing application: Preparation and characterization. *Mater. Sci. Eng. C* **2017**, *72*, 543–550. [[CrossRef](#)] [[PubMed](#)]
39. Zheng, H.; Wang, L. Banana Peel Carbon that Containing Functional Groups Applied to the Selective Adsorption of Au(III) from Waste Printed Circuit Boards. *Soft Nanosci. Lett.* **2013**, *3*, 29–36. [[CrossRef](#)]
40. Lingegowda, D.C.; Kumar, J.K.; Prasad, A.G.D.; Zarei, M.; Gopal, S. Ftir Spectroscopic Studies on Cleome Gynandra–Comparative. *Rom. J. Biophys.* **2012**, *22*, 137–143.
41. Al Aani, S.; Wright, C.J.; Hilal, N. Investigation of UF membranes fouling and potentials as pre-treatment step in desalination and surface water applications. *Desalination* **2018**, *432*, 115–127. [[CrossRef](#)]
42. Shakak, M.; Rezaee, R.; Maleki, A.; Jafari, A.; Safari, M.; Shahmoradi, B.; Daraei, H.; Lee, S.-M. Synthesis and characterization of nanocomposite ultrafiltration membrane (PSF/PVP/SiO<sub>2</sub>) and performance evaluation for the removal of amoxicillin from aqueous solutions. *Environ. Technol. Innov.* **2020**, *17*, 100529. [[CrossRef](#)]
43. Ismail, A.; Ng, B.; Rahman, W.A. Effects of shear rate and forced convection residence time on asymmetric polysulfone membranes structure and gas separation performance. *Sep. Purif. Technol.* **2003**, *33*, 255–272. [[CrossRef](#)]

44. Vatanpour, V.; Madaeni, S.S.; Moradian, R.; Zinadini, S.; Astinchap, B. Fabrication and characterization of novel antifouling nanofiltration membrane prepared from oxidized multiwalled carbon nanotube/polyethersulfone nanocomposite. *J. Membr. Sci.* **2011**, *375*, 284–294. [[CrossRef](#)]
45. Zinadini, S.; Zinatizadeh, A.A.; Rahimi, M.; Vatanpour, V.; Zangeneh, H. Preparation of a novel antifouling mixed matrix PES membrane by embedding graphene oxide nanoplates. *J. Membr. Sci.* **2014**, *453*, 292–301. [[CrossRef](#)]
46. Kusuma, N.C.; Purwanto, M.; Sudrajat, M.A.; Jaafar, J.; Othman, M.H.D.; Aziz, M.H.A.; Raharjo, Y.; Qtaishat, M.R. Fabrication and characterization of modified PVDF hollow fiber membrane coated with hydrophobic surface modifying macromolecules for desalination application. *J. Environ. Chem. Eng.* **2021**, *9*, 105582. [[CrossRef](#)]
47. Kumar, A.; Nayak, K.; Münch, A.; Uhlmann, P.; Fery, A.; Tripathi, B. Mussel primed grafted zwitterionic phosphorylcholine based superhydrophilic/underwater superoleophobic antifouling membranes for oil-water separation. *Sep. Purif. Technol.* **2022**, *290*, 120887. [[CrossRef](#)]
48. Tahazadeh, S.; Mohammadi, T.; Tofighy, M.A.; Khanlari, S.; Karimi, H.; Emrooz, H.B.M. Development of cellulose acetate/metal-organic framework derived porous carbon adsorptive membrane for dye removal applications. *J. Membr. Sci.* **2021**, *638*, 119692. [[CrossRef](#)]
49. Ma, J.; Guo, X.; Ying, Y.; Liu, D.; Zhong, C. Composite ultrafiltration membrane tailored by MOF@GO with highly improved water purification performance. *Chem. Eng. J.* **2017**, *313*, 890–898. [[CrossRef](#)]
50. Jamed, M.J.; Alanezi, A.A.; Alsahy, Q.F. Effects of embedding functionalized multi-walled carbon nanotubes and alumina on the direct contact poly(vinylidene fluoride-co-hexafluoropropylene) membrane distillation performance. *Chem. Eng. Commun.* **2019**, *206*, 1035–1057. [[CrossRef](#)]
51. Alfalahy, H.N.; Al-Jubouri, S.M. Preparation and application of polyethersulfone ultrafiltration membrane incorporating NaX zeolite for lead ions removal from aqueous solutions. *Desalination Water Treat.* **2022**, *248*, 149–162. [[CrossRef](#)]
52. Rizqi, R.A.; Hartono, Y.V.; Shalahuddin, I.; Nugroho, W.A.; Bilad, M.R.; Arif, C.; Wibisono, Y. Green synthesis of polyvinylidene fluoride ultrafiltration membrane with upgraded hydrophilicity. *Results Mater.* **2023**, *19*, 100417. [[CrossRef](#)]
53. Li, H.; Shi, W.; Zeng, X.; Huang, S.; Zhang, H.; Qin, X. Improved desalination properties of hydrophobic GO-incorporated PVDF electrospun nanofibrous composites for vacuum membrane distillation. *Sep. Purif. Technol.* **2020**, *230*, 115889. [[CrossRef](#)]
54. Tomietto, P.; Russo, F.; Galiano, F.; Loulergue, P.; Salerno, S.; Paugam, L.; Audic, J.-L.; De Bartolo, L.; Figoli, A. Sustainable fabrication and pervaporation application of bio-based membranes: Combining a polyhydroxyalkanoate (PHA) as biopolymer and Cyrene™ as green solvent. *J. Membr. Sci.* **2022**, *643*, 120061. [[CrossRef](#)]
55. Pan, J.; Zhang, F.; Wang, Z.; Sun, S.-P.; Cui, Z.; Jin, W.; Bamaga, O.; Abulkhair, H.; Albeirutty, M.; Drioli, E. Enhanced anti-wetting and anti-fouling properties of composite PFPE/PVDF membrane in vacuum membrane distillation. *Sep. Purif. Technol.* **2022**, *282*, 120084. [[CrossRef](#)]
56. Kadhim, R.J.; Al-Ani, F.H.; Al-Shaeli, M.; Alsahy, Q.F.; Figoli, A. Removal of dyes using graphene oxide (Go) mixed matrix membranes. *Membranes* **2020**, *10*, 366. [[CrossRef](#)] [[PubMed](#)]
57. Najjar, A.; Sabri, S.; Al-Gaashani, R.; Atieh, M.A.; Kochkodan, V. Antibiofouling performance by polyethersulfone membranes cast with oxidized multiwalled carbon nanotubes and arabic gum. *Membranes* **2019**, *9*, 32. [[CrossRef](#)] [[PubMed](#)]
58. Li, W.; Wang, X.; He, M.; Zhang, Z.; Chen, J.; Yang, G. Fabrication of high-performance nanofiltration membranes by using sulfated cellulose nanofibril as the intermediate support layer. *Desalination* **2022**, *532*, 115741. [[CrossRef](#)]
59. Matindi, C.N.; Hu, M.; Kadanyo, S.; Ly, Q.V.; Gumbi, N.N.; Dlamini, D.S.; Li, J.; Hu, Y.; Cui, Z.; Li, J. Tailoring the morphology of polyethersulfone/sulfonated polysulfone ultrafiltration membranes for highly efficient separation of oil-in-water emulsions using TiO<sub>2</sub> nanoparticles. *J. Membr. Sci.* **2021**, *620*, 118868. [[CrossRef](#)]
60. Mahmoudi, E.; Ng, L.Y.; Ang, W.L.; Teow, Y.H.; Mohammad, A.W. Improving membrane bioreactor performance through the synergistic effect of silver-decorated graphene oxide in composite membranes. *J. Water Process. Eng.* **2020**, *34*, 101169. [[CrossRef](#)]
61. Al-Timimi, D.A.H.; Alsahy, Q.F.; AbdulRazak, A.A.; Drioli, E. Novel polyether sulfone/polyethylenimine grafted nano-silica nanocomposite membranes: Interaction mechanism and ultrafiltration performance. *J. Membr. Sci.* **2022**, *659*, 120784. [[CrossRef](#)]
62. Huang, A.; Liu, F.; Cui, Z.; Song, X.; Geng, L.; Wang, H.; Peng, X. Novel PTFE/CNT composite nanofiber membranes with enhanced mechanical, crystalline, conductive, and dielectric properties fabricated by emulsion electrospinning and sintering. *Compos. Sci. Technol.* **2021**, *214*, 108980. [[CrossRef](#)]
63. Han, Y.; Shi, J.; Mao, L.; Wang, Z.; Zhang, L. Improvement of Compatibility and Mechanical Performances of PLA/PBAT Composites with Epoxidized Soybean Oil as Compatibilizer. *Ind. Eng. Chem. Res.* **2020**, *59*, 21779–21790. [[CrossRef](#)]
64. Dlamini, D.S.; Mamba, B.B.; Li, J. The role of nanoparticles in the performance of nano-enabled composite membranes—A critical scientific perspective. *Sci. Total. Environ.* **2019**, *656*, 723–731. [[CrossRef](#)] [[PubMed](#)]
65. Khalid, F.; Roy, A.S.; Parveen, A.; Castro-Muñoz, R. Fabrication of the cross-linked PVA/TiO<sub>2</sub>/C nanocomposite membrane for alkaline direct methanol fuel cells. *Mater. Sci. Eng. B* **2024**, *299*, 116929. [[CrossRef](#)]
66. Nasrollahi, N.; Aber, S.; Vatanpour, V.; Mahmoodi, N.M. Development of hydrophilic microporous PES ultrafiltration membrane containing CuO nanoparticles with improved antifouling and separation performance. *Mater. Chem. Phys.* **2019**, *222*, 338–350. [[CrossRef](#)]
67. Wen, Y.; Yuan, J.; Ma, X.; Wang, S.; Liu, Y. Polymeric nanocomposite membranes for water treatment: A review. *Environ. Chem. Lett.* **2019**, *17*, 1539–1551. [[CrossRef](#)]

68. Abbas, T.K.; Rashid, K.T.; Alsahy, Q.F. NaY zeolite-polyethersulfone-modified membranes for the removal of cesium-137 from liquid radioactive waste. *Chem. Eng. Res. Des.* **2022**, *179*, 535–548. [[CrossRef](#)]
69. Hosseini, S.; Afshari, M.; Fazlali, A.; Farahani, S.K.; Bandedhali, S.; Van der Bruggen, B.; Bagheripour, E. Mixed matrix PES-based nanofiltration membrane decorated by (Fe<sub>3</sub>O<sub>4</sub>-polyvinylpyrrolidone) composite nanoparticles with intensified antifouling and separation characteristics. *Chem. Eng. Res. Des.* **2019**, *147*, 390–398. [[CrossRef](#)]
70. Najjar, A.; Sabri, S.; Al-Gaashani, R.; Kochkodan, V.; Atieh, M.A. Enhanced fouling resistance and antibacterial properties of novel graphene oxide-arabic gum polyethersulfone membranes. *Appl. Sci.* **2019**, *9*, 513. [[CrossRef](#)]
71. Prince, J.; Bhuvana, S.; Anbharasi, V.; Ayyanar, N.; Boodhoo, K.; Singh, G. Ultra-wetting graphene-based PES ultrafiltration membrane—A novel approach for successful oil-water separation. *Water Res.* **2016**, *103*, 311–318. [[CrossRef](#)]
72. Zhu, Y.; Zhang, F.; Wang, D.; Pei, X.F.; Zhang, W.; Jin, J. A novel zwitterionic polyelectrolyte grafted PVDF membrane for thoroughly separating oil from water with ultrahigh efficiency. *J. Mater. Chem. A* **2013**, *1*, 5758–5765. [[CrossRef](#)]
73. Matindi, C.N.; Kadanyo, S.; Liu, G.; Hu, M.; Hu, Y.; Cui, Z.; Ma, X.; Yan, F.; He, B.; Li, J. Hydrophilic polyethyleneimine-TiO<sub>2</sub> hybrid layer on polyethersulfone/sulfonated polysulfone blend membrane with antifouling characteristics for the effective separation of oil-in-water emulsions. *J. Water Process. Eng.* **2022**, *49*, 102982. [[CrossRef](#)]
74. Motsa, M.M.; Msagati, T.A.M.; Thwala, J.M.; Mamba, B.B. Polypropylene-zeolite polymer composites for water purification: Synthesis, characterisation and application. *Desalination Water Treat.* **2015**, *53*, 2604–2612. [[CrossRef](#)]
75. Erragued, R.; Sharma, M.; Costa, C.; Bouaziz, M.; Gando-Ferreira, L.M. Novel polyethersulfone mixed matrix adsorptive nanofiltration membrane fabricated from embedding zinc oxide coated by polyaniline. *J. Environ. Chem. Eng.* **2023**, *11*, 111607. [[CrossRef](#)]
76. Mohammadi, T.; Esmaeilifar, A. Wastewater treatment of a vegetable oil factory by a hybrid ultrafiltration-activated carbon process. *J. Membr. Sci.* **2005**, *254*, 129–137. [[CrossRef](#)]
77. Hussain, A.; Al-Yaari, M. Development of polymeric membranes for oil/water separation. *Membranes* **2021**, *11*, 42. [[CrossRef](#)]
78. Zarghami, S.; Mohammadi, T.; Sadrzadeh, M. Preparation, characterization and fouling analysis of in-air hydrophilic/underwater oleophobic bio-inspired polydopamine coated PES membranes for oily wastewater treatment. *J. Membr. Sci.* **2019**, *582*, 402–413. [[CrossRef](#)]
79. Al-Anzi, B.S.; Siang, O.C. Recent developments of carbon based nanomaterials and membranes for oily wastewater treatment. *RSC Adv.* **2017**, *7*, 20981–20994. [[CrossRef](#)]
80. Hua, F.L.; Tsang, Y.F.; Wang, Y.J.; Chan, S.Y.; Chua, H.; Sin, S.N. Performance study of ceramic microfiltration membrane for oily wastewater treatment. *Chem. Eng. J.* **2007**, *128*, 169–175. [[CrossRef](#)]
81. Ho, K.; Teow, Y.; Ang, W.; Mohammad, A. Novel GO/OMWCNTs mixed-matrix membrane with enhanced antifouling property for palm oil mill effluent treatment. *Sep. Purif. Technol.* **2017**, *177*, 337–349. [[CrossRef](#)]
82. Biron, D.D.S.; Zeni, M.; Bergmann, C.P.; Dos Santos, V. Analysis of composite membranes in the separation of emulsions sunflower oil/water. *Mater. Res.* **2017**, *20*, 843–852. [[CrossRef](#)]
83. Lim, Y.J.; Lee, S.M.; Wang, R.; Lee, J. Emerging materials to prepare mixed matrix membranes for pollutant removal in water. *Membranes* **2021**, *11*, 508. [[CrossRef](#)] [[PubMed](#)]
84. Kebria, M.R.S.; Jahanshahi, M.; Rahimpour, A. SiO<sub>2</sub> modified polyethyleneimine-based nanofiltration membranes for dye removal from aqueous and organic solutions. *Desalination* **2015**, *367*, 255–264. [[CrossRef](#)]
85. Koo, C.H.; Mohammad, A.W.; Suja', F.; Talib, M.Z.M. Review of the effect of selected physicochemical factors on membrane fouling propensity based on fouling indices. *Desalination* **2012**, *287*, 167–177. [[CrossRef](#)]
86. Ng, L.Y.; Mohammad, A.W.; Leo, C.P.; Hilal, N. Polymeric membranes incorporated with metal/metal oxide nanoparticles: A comprehensive review. *Desalination* **2013**, *308*, 15–33. [[CrossRef](#)]
87. Yang, X.; He, Y.; Zeng, G.; Chen, X.; Shi, H.; Qing, D.; Li, F.; Chen, Q. Bio-inspired method for preparation of multiwall carbon nanotubes decorated superhydrophilic poly(vinylidene fluoride) membrane for oil/water emulsion separation. *Chem. Eng. J.* **2017**, *321*, 245–256. [[CrossRef](#)]
88. Liu, Y.; Su, Y.; Cao, J.; Guan, J.; Zhang, R.; He, M.; Fan, L.; Zhang, Q.; Jiang, Z. Antifouling, high-flux oil/water separation carbon nanotube membranes by polymer-mediated surface charging and hydrophilization. *J. Membr. Sci.* **2017**, *542*, 254–263. [[CrossRef](#)]
89. Nasrollahi, N.; Vatanpour, V.; Aber, S.; Mahmoodi, N.M. Preparation and characterization of a novel polyethersulfone (PES) ultrafiltration membrane modified with a CuO/ZnO nanocomposite to improve permeability and antifouling properties. *Sep. Purif. Technol.* **2018**, *192*, 369–382. [[CrossRef](#)]
90. Yu, H.; Liu, H.; Yuan, X.; Ding, W.; Li, Y.; Wang, J. Separation of oil-water emulsion and adsorption of Cu(II) on a chitosan-cellulose acetate-TiO<sub>2</sub> based membrane. *Chemosphere* **2019**, *235*, 239–247. [[CrossRef](#)]
91. Sadiq, A.J.; Shabeeb, K.M.; Khalil, B.I.; Alsahy, Q.F. Effect of embedding MWCNT-g-GO with PVC on the performance of PVC membranes for oily wastewater treatment. *Chem. Eng. Commun.* **2020**, *207*, 733–750. [[CrossRef](#)]
92. Al-Ani, F.H.; Alsahy, Q.F.; Raheem, R.S.; Rashid, K.T.; Figoli, A. Experimental investigation of the effect of implanting tio2-nps on pvc for long-term uf membrane performance to treat refinery wastewater. *Membranes* **2020**, *10*, 77. [[CrossRef](#)]
93. Zhang, N.; Yang, N.; Zhang, L.; Jiang, B.; Sun, Y.; Ma, J.; Cheng, K.; Peng, F. Facile hydrophilic modification of PVDF membrane with Ag/EGCG decorated micro/nanostructural surface for efficient oil-in-water emulsion separation. *Chem. Eng. J.* **2020**, *402*, 126200. [[CrossRef](#)]

94. Kazemi, F.; Jafarzadeh, Y.; Masoumi, S.; Rostamizadeh, M. Oil-in-water emulsion separation by PVC membranes embedded with GO-ZnO nanoparticles. *J. Environ. Chem. Eng.* **2021**, *9*, 104992. [[CrossRef](#)]
95. Yang, J.; Cui, J.; Xie, A.; Dai, J.; Li, C.; Yan, Y. Facile preparation of superhydrophilic/underwater superoleophobic cellulose membrane with CaCO<sub>3</sub> particles for oil/water separation. *Colloids Surf. A Physicochem. Eng. Asp.* **2021**, *608*, 125583. [[CrossRef](#)]
96. Al-Jadir, T.; Alardhi, S.M.; Alheety, M.A.; Najim, A.A.; Salih, I.K.; Al-Furaiji, M.; Alsalhy, Q.F. Fabrication and Characterization of Polyphenylsulfone/Titanium Oxide Nanocomposite Membranes for Oily Wastewater Treatment. *J. Ecol. Eng.* **2022**, *23*, 1–13. [[CrossRef](#)]
97. Ahmad, T.; Liu, X.; Guria, C. Preparation of polyvinyl chloride (PVC) membrane blended with acrylamide grafted bentonite for oily water treatment. *Chemosphere* **2023**, *310*, 136840. [[CrossRef](#)]
98. Ghorbani, M.; Vakili, M.H.; Ameri, E. Fabrication and evaluation of a biopolymer-based nanocomposite membrane for oily wastewater treatment. *Mater. Today Commun.* **2021**, *28*, 102560. [[CrossRef](#)]
99. Qin, Y.; Shen, H.; Han, L.; Zhu, Z.; Pan, F.; Yang, S.; Yin, X. Mechanically Robust Janus Poly(lactic acid) Hybrid Fibrous Membranes toward Highly Efficient Switchable Separation of Surfactant-Stabilized Oil/Water Emulsions. *ACS Appl. Mater. Interfaces* **2020**, *12*, 50879–50888. [[CrossRef](#)]

**Disclaimer/Publisher’s Note:** The statements, opinions and data contained in all publications are solely those of the individual author(s) and contributor(s) and not of MDPI and/or the editor(s). MDPI and/or the editor(s) disclaim responsibility for any injury to people or property resulting from any ideas, methods, instructions or products referred to in the content.